

# ADAPT: An Autonomous Forklift for Construction Site Operation<sup>\*</sup>

Johannes Huemer<sup>a,1</sup>, Markus Murschitz<sup>a,1</sup>, Matthias Schörghuber<sup>a</sup>, Lukas Reisinger<sup>a</sup>, Thomas Kadiofsky<sup>a</sup>, Christoph Weidinger<sup>a</sup>, Mario Niedermeyer<sup>a</sup>, Benedikt Widy<sup>a</sup>, Marcel Zeilinger<sup>a</sup>, Csaba Beleznai<sup>a</sup>, Tobias Glück<sup>a</sup>, Andreas Kugi<sup>a,b</sup>, Patrik Zips<sup>a,1,\*</sup>

<sup>a</sup>AIT Austrian Institute of Technology GmbH, Center for Vision, Automation and Control, Giefinggasse 4, 1210, Vienna, Austria

<sup>b</sup>Technische Universität Wien, Automation and Control Institute, Gußhausstrasse 27-29, 1040, Vienna, Austria

## Abstract

Efficient material logistics play a critical role in controlling costs and schedules in the construction industry. However, manual material handling remains prone to inefficiencies, delays, and safety risks. Autonomous forklifts offer a promising solution to streamline on-site logistics, reducing reliance on human operators and mitigating labor shortages. This paper presents the development and evaluation of the Autonomous Dynamic All-terrain Pallet Transporter (ADAPT), a fully autonomous off-road forklift designed for construction environments. Unlike structured warehouse settings, construction sites pose significant challenges, including dynamic obstacles, unstructured terrain, and varying weather conditions. To address these challenges, our system integrates AI-driven perception techniques with traditional approaches for decision making, planning, and control, enabling reliable operation in complex environments. We validate the system through extensive real-world testing, comparing its long-term performance against an experienced human operator across various weather conditions. We also provide a comprehensive analysis of challenges and key lessons learned, contributing to the advancement of autonomous heavy machinery. Our findings demonstrate that autonomous outdoor forklifts can operate near human-level performance, offering a viable path toward safer and more efficient construction logistics.

## 1. Introduction

Streamlined logistics are critical to managing both costs and timelines in the construction industry. Studies indicate that materials represent more than half of the total construction costs and influence up to 80% of the project schedules [1]. A well-orchestrated on-site logistics, including resource delivery, storage and distribution [2], ensures that resources are available when and where they are needed, reducing delays and costs [3]. Numerous studies have identified inefficient on-site material management as a major contributor to project delays, see [4].

Digitalization and automation has the potential to revolutionize construction logistics. While digitalization allows optimal planning and tracking of materials, automation of machinery ensures fluid and timely material flow operation on the construction site. A multitude of reliable and flexible autonomous machines may be utilized to service the site in pull, push as well as just in time deliveries. In particular, forklifts are easy to bring to construction sites, even in large numbers, and are flexible in operation, which makes them well suited for ground-based material flow, lifting the workload of restricted cranes. When seamlessly integrated into the construction process through IT services, forklifts

can greatly improve site efficiency by minimizing downtime, streamlined material handling, and preventing both equipment idleness and worker delays [5]. With the increasing shortage of skilled workers, the rough and dangerous working conditions, and the required increase in efficiency and decrease of errors, automation of these machines seems mandatory in the near future.



Figure 1: The autonomous off-road forklift ADAPT (Autonomous Dynamic All-terrain Pallet Transporter) demonstrating precision pallet loading onto a truck during a field demonstration. Throughout the development phase, the vehicle was equipped with additional hardware for testing outdoor sensor systems.

<sup>\*</sup>This document is the result of the research project AWARD funded by the European H2020 program, No. 101006817.

<sup>\*</sup>Corresponding author.

E-mail address: patrik.zips@ait.ac.at (P. Zips).

<sup>1</sup>These authors contributed equally to this work.

However, the dynamic and unstructured environments of construction sites and the variable weather conditions pose significant challenges for automation. Unlike the controlled settings of autonomous warehouses, construction sites require flexible route planning and operation to navigate unpredictable terrains and obstacles. Safety is another paramount aspect, as 6% of total construction costs are due to accidents and one third of all fatalities at construction sites are caused by material handling equipment [6]. Despite advances in automation, there is a notable scarcity of autonomous machines capable of long-term operation in outdoor environments. Current solutions often fail in terms of robustness and adaptability, particularly when it comes to tasks such as unloading and loading full pallets from trucks. This gap underscores the need for innovative systems that can seamlessly integrate into the demanding conditions of construction sites.

This paper presents the autonomous off-road forklift ADAPT (Autonomous Dynamic All-terrain Pallet Transporter), depicted in Figure 1, addressing the critical need for enhanced material handling solutions in construction. The scenario under consideration is a typical construction site that is not designed for autonomous operation. Predefined structures, guiding systems, or designated high-precision cargo locations are not required. Using advanced task and motion planning, purely synthetically trained geometry-based pallet detection, collision avoidance, and a new factor-graph-based joint vehicle localization and pallet mapping approach, our system aims to provide a reliable and efficient alternative to manual operation in this environment. The vehicle localization and pallet mapping approach is a specialized variant of traditional Simultaneous Localization and Mapping (SLAM) methods, specifically designed for manipulation tasks. Unlike most SLAM techniques, which rely on natural features (mid-level) or raw sensor data (low-level), this approach operates at a higher level by utilizing object poses—specifically, pallet locations. The overall approach and technology are designed to ensure mandatory adaptability to dynamic construction site conditions while maintaining robust and reliable operation. This is achieved through a combination of novel AI-based approaches (e.g., pallet detection) and classical physics-driven methodologies for task management, motion planning, and control. The use of primarily cost-effective sensors ensures affordability, while extensive real-world testing in various weather conditions validates the system’s performance. Through a comparative analysis with an experienced human operator, we demonstrate the potential of our automated forklift to give a realistic estimate of the performance and viability of autonomous machines in the coming years.

### 1.1. Contribution

This paper presents a comprehensive system overview for an autonomous forklift for flexible outdoor operation. This includes hardware modifications and complete software integration for perception, planning and control spe-

cialized to the needs of construction sites. The main contributions are:

- Development and validation of an autonomous forklift system capable of loading and unloading operations in unstructured outdoor environments, demonstrating near-human performance across varied weather conditions, particularly robust operation under low to medium rainfall.
- Design and implementation of a novel factor-graph-based joint optimization framework for precise vehicle localization and pallet mapping, specifically engineered to enhance object manipulation accuracy in pallet loading tasks.
- Introduction of an innovative fork contact measurement system utilizing pressure feedback, significantly enhancing manipulation robustness and operational safety while maintaining cost-effectiveness and implementation simplicity.
- Comprehensive performance evaluation comparing the autonomous system against an expert human operator with over 20 years of experience, including detailed quantitative analysis of operational efficiency, system robustness, and the frequency and severity of required human interventions during extended autonomous operation.

Unlike many publications that focus solely on successful outcomes and scenarios, we provide a comprehensive section highlighting problems and key lessons learned from the long-term development and testing of autonomous machines. We believe that this will aid the scientific and engineering community in accelerating advances in heavy machine automation and, in the long run, contribute to safer and more reliable systems.

### 1.2. Article structure

The remainder of this paper is organized as follows. Section 2 presents a review of recent advances in autonomous outdoor machinery and related research in robotic material handling. Section 3 provides an overview of the proposed system, including its hardware and software components. The perception system, responsible for environment sensing, obstacle detection, and localization, is described in Section 4. Section 5 details the planning and control strategies used for autonomous navigation and load handling. In Section 6, we evaluate the system’s performance compared to an expert operator through experiments conducted in real-world outdoor environments and provide development and testing insights. Finally, Section 7 concludes the paper and discusses potential directions for future work. An overview of the system components and the corresponding sections is sketched in Fig. 2.

## 2. Related Work

While automated manipulation and logistics have reached commercial readiness in structured indoor environments,

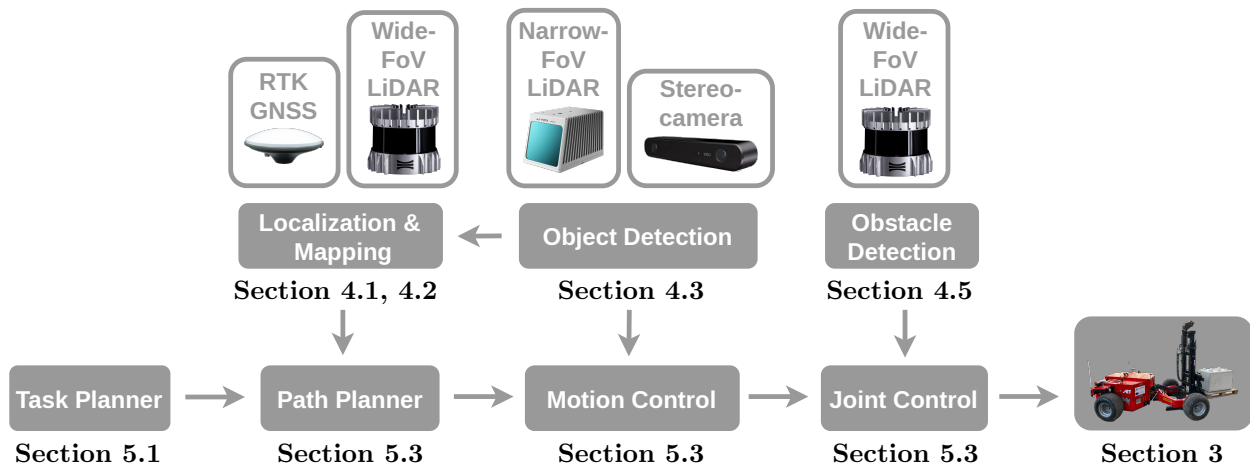


Figure 2: System architecture of the proposed autonomous forklift, illustrating the hierarchical organization of key components essential for autonomous operation. The diagram depicts high-level information pathways and data flow between integrated sensors and specialized processing modules throughout the system. Relevant section references are provided alongside each major component, directing readers to corresponding detailed descriptions within the manuscript.

automated machines in rough, outdoor environments remain primarily in the research phase. Nevertheless, recent years have produced several promising prototypes. The HEAP platform [7] combines navigation and manipulation capabilities in a legged excavator. This outstanding research platform has demonstrated various tasks including excavation, dry-wall construction with natural stones, and forestry operations using both classical control techniques and novel AI approaches. Similarly, the Harveri platform [8] employs comparable technologies to harvest trees in challenging environments.

An automated logistics yard machine [9] was introduced for mixed operations with both manual and automated vehicles. The machine’s core capabilities—driving in open spaces and precise docking for trailer pick-up—closely resemble forklift operations. However, detailed technical information about the automation system remains unavailable.

Over the past two decades, several research platforms for autonomous forklift solutions have been published. Earlier work [10] explored vision-based handling tasks for autonomous outdoor forklifts, particularly focusing on vision systems for transporting molten aluminum in the metal industry. Another study [11] presented a system configuration for autonomous forklift operation that incorporated vision, laser range finders, sonar, and other sensors. This research analyzed the kinematics of a spin-turn mechanism and established essential system equations for path following based on time-varying feedback control law. However, in stark contrast to our work, their evaluation merely demonstrated the basic functionality of path following without presenting comprehensive real-world evaluations of loading success.

To our knowledge, only two similar scientific publications [12, 13] focus on autonomous forklifts in outdoor operation. The first [12] primarily emphasized motion planning with an anytime approach and explored new in-

teraction modalities with human workers, such as voice commands. This work used trained AI only for object reacquisition after manual annotation of a single frame. Although it presented the robustness of the path planning, it did not provide a robustness or performance analysis of the complete loading cycle. Similarly, the second study [13] concentrated on the successful unloading of a specific pallet type from a truck, without offering comparative analysis against the performance of the human operator.

Another promising platform has been presented by the Linde group and their scientific collaborators, featuring counterbalanced forklifts capable of operating in both indoor and outdoor environments [14]. This research emphasized cooperative behavior through real-time information exchange, handling of inclines and gradients, and management of weather influences. The work highlighted the necessity for enhanced performance in outdoor settings, including the ability to navigate inclines and adapt to varying weather conditions. However, no scientific publication detailing technical specifications or evaluation results is currently available.

### 2.1. Localization, Mapping, and Traversability

To enable a system to operate in unfamiliar environments, a common approach is to use variants of SLAM (Simultaneous Localization and Mapping) [15]. SLAM is a technique that simultaneously constructs a map of an unknown environment while tracking the agent’s location within that environment, and has been extensively studied and applied in robotics applications [16, 17]. For autonomous unmanned forklifts, the SLAM method presented in [18] demonstrates robust operation in real-world, large-scale, and unstructured warehouse environments by employing a stereo-camera-based approach. This method achieves efficiency and robustness through a combination of direct (pixel-based) and indirect (feature-based) SLAM,

focusing primarily on mapping indoor environments in mostly static settings.

Environment mapping is even more crucial for autonomous truck-mounted forklifts operating in unfamiliar construction sites. It serves as the foundation for traversability analysis and downstream path planning, enabling safe and efficient navigation. While mapping robot environments has been extensively studied over past decades, significant challenges remain in achieving human-like scene understanding—essential for enabling robots to navigate unstructured environments safely. Simple 2D occupancy grids may suffice for structured indoor spaces, but complex terrains require richer representations. The work [19] introduced a pioneering approach to address memory and runtime efficiency challenges in 3D occupancy maps, which has since been enhanced by methods such as spatio-temporal voxel layers [20] and VDB [21]. Other popular representations for 3D mapping include point clouds [22] and implicit representations [23, 24, 25].

Although these methods emphasize geometric reconstruction, [26] provides a comprehensive survey on scene understanding via traversability estimation and terrain classification. This survey explores the application of various proprioceptive and exteroceptive sensors across nonlearning-based, traditional learning-based, and deep learning-based approaches, highlighting their effectiveness in enhancing navigation capabilities in diverse environments. When multiple sensors are used in a mapping approach, it is common to implement certain aspects of sensor fusion and state estimation together with SLAM. For comparative overviews on sensor fusion, see [27] and [28] for a focus on autonomous driving applications.

An elegant unified approach is to use algorithms based on factor graphs [29]. Although filter-based techniques perform well in state estimation [30, 31], in the SLAM context, factor graphs have become the standard methodology [17, 32]. They allow for an efficient representation of not only the sensor fusion functionality but also the occurrence of signals over time. The frequency of these signals can vary in such systems, and algorithms exist that can solve for the most probable state of the system given a series of measurements, subject to the system’s constraints (i.e., maximum a posteriori likelihood estimation). A notable algorithm for solving such problems is iSAM2 [33], which uses factor graphs as its foundational framework while focusing on efficient incremental updates over time. The variant of SLAM that we present in this paper employs the factor graph method not only to locate the forklift, but also to determine the poses of the pallet in a joint optimization problem.

## 2.2. Pallet Pose Estimation

Automated pallet manipulation requires the estimation of the 3D pallet pose with respect to the vision sensor. As we focus on a specific pallet type of known size and geometry (Euro-pallet), the vision task becomes *instance-level* pose estimation. To tackle this task, common pose-

aware pallet detection approaches adopt either geometric cues from depth data or are based on visual appearance. *Geometric schemes* typically focus on 2D structure templates [34] or perform geometric fitting on point-cloud data from stereo [35], Time-of-Flight or LiDAR sensing [13]. In the presence of clutter and partial occlusions, however, geometric analysis schemes inherently become ambiguous. *Appearance-based* neural representations, sometimes complemented by depth in the form of RGB-D images, yield highly object-specific detectors, as demonstrated for 3D pose estimation in recent challenges [36]. Especially occlusion-robust local key-point representations [37, 38] offer accurate pose estimation results in high-resolution and semantically rich RGB or RGB-D data spaces. The work [39] introduces a pallet detection method based on the concept of *Front Face Shots*, which represent the access side of the pallets, where the pockets are. Their approach demonstrates that by combining a machine learning-based object detector with a kernel-based regression method, an accurate 6D pose can be computed, even for previously unseen pallet appearances.

Our employed pallet pose estimation scheme [40] exclusively relies on depth data to reduce object variations only to geometric traits. Furthermore, as a distinctive feature compared to most state-of-the-art, we only use stereo depth computed on synthetic image pairs for training, to generate an infinite diversity of view configurations with a narrow sim-to-real gap.

## 2.3. Task Planning

Task Planning is essential for automating utility machinery, particularly in complex load manipulation tasks such as pallet handling. It involves high-level decision-making and sequencing of operations. Early approaches relied on finite state machines (FSMs) but evolved into hierarchical behavior trees for greater modularity and reactivity [41]. Similarly, the autonomous system under evaluation employs a modular behavior tree implementation to efficiently manage task execution. More recently, integrated Task and Motion Planning (TAMP) methods have emerged [42], combining symbolic reasoning with motion feasibility checks [43] or hierarchical architectures that leverage Linear Temporal Logic (LTL) for high-level planning and reactive behavior trees for low-level control [44]. Learning-based methods are being explored to infer planning domains from data, reducing the reliance on manually defined preconditions [45]. Recent developments have deployed LLMs for task planning. Although LLMs excel at processing natural language and common sense reasoning, directly translating abstract language inputs into executable plans is problematic due to their limited grounding in physical environments and inability to reason over complex task sequences [46]. LLMs struggle with the physical understanding of actions and fail to manage long-term dependencies in multiple steps, limiting their applicability to planning real-world tasks [47]. Recent research has explored the integration of LLMs with



classical planners to capitalize on the language understanding of LLMs while leveraging the precision of PDDL-based planning [48, 49]. This hybrid approach improves the decision making capabilities of autonomous agents, allowing them to process natural language instructions and generate actionable plans using PDDL-based frameworks [50, 51]. However, no reliable long-term operation is yet feasible.

#### 2.4. Motion Planning and Control

Motion planning and control ensure task feasibility, forming an adaptive feedback loop for execution. In the context of vehicles, motion planning must account for non-holonomic constraints such as limited turning radii and restricted maneuverability [52, 53]. One such constraint arises from the articulation of the center, a common feature in heavy-duty vehicles, which significantly influences the kinematic behavior.

Various approaches have been developed to address these challenges. A Goal-Directed Rapidly exploring Random Tree (RRT) with multi-step refinement has been proposed for articulated construction machines [54]. Similarly, an extended Reeds-Sheep algorithm has been applied to wheel loader path planning [55]. A modified bug-like algorithm, integrated with Model Predictive Control (MPC) to ensure smoother trajectory execution, was proposed in [56]. Additionally, offline motion primitive generation combined with online receding-horizon planning has been successfully applied to tree harvester vehicles [57]. Application-focused path planning for yard automation was proposed in [58].

For tracking and control, a variant of the pure-pursuit method for the tracking of the path of articulated vehicles was introduced in [57], while another tracking controller has been specifically developed for articulated drum rollers that navigate construction sites [59].

Our navigation approach employs the well-established Hybrid A\* planner with a Reeds-Shepp configuration [60] by introducing an analytic conversion between car-like and articulated vehicles for constant curvature driving. This path planning is complemented by a Lyapunov-based path tracking controller similar to [59].

Beyond collision-free navigation, precise pallet docking is crucial for autonomous forklifts. Successful docking relies on accurate pallet pose estimation, achieved through vision-based systems, laser range finders, or hybrid sensor fusion approaches. The literature explores various motion planning techniques for this task, including geometric-based path generation [13, 61] and dynamic-based planning methods [62]. In addition, advanced control strategies, such as visual servoing [63], have been used to enhance the accuracy of jacking. Some methods also consider pallet inclination during insertion [64], improving adaptability and robustness in unstructured environments.

For the system presented in this paper, the docking approach is based on visual servoing, integrating depth-camera and LiDAR measurements to achieve precise pallet engagement under varied environmental conditions.

### 3. System Design

This section describes ADAPT, including the vehicle platform it is based on, the hardware modifications necessary for automation, and an overview of the key software components.

#### 3.1. Vehicle Platform

ADAPT is built on the Palfinger BM154 truck-mounted platform. Unlike common warehouse forklifts, this platform is remotely controlled, which eliminates the need for an operator seat. Its foldable design allows it to be stored beneath a truck’s cargo area, making it an ideal solution for delivering goods to environments without established infrastructure. The vehicle is widely used in challenging operational settings in multiple industries, including the delivery of construction material to the worksites, the transportation of agricultural equipment and landscaping supplies, the logistics of beverages, and civil protection and disaster management.

Table 1: Specifications of the Palfinger BM154 platform.

<b>Safe Working Load</b>	1500kg @ 0.6m
<b>Lift Height</b>	2.85m
<b>Weight</b>	Approx. 1500kg
<b>Engine</b>	3-cylinder Diesel, 18.8kW
<b>Drive System</b>	Hydrostatic 4-wheel drive

Table 1 lists the main technical specifications of the BM154. The platform’s primary strengths lie in its advanced all-terrain capabilities, enabled by an all-wheel drive system and its center articulated steering with 3 rotational degrees of freedom, see Figure 3a. These features allow to navigate in uneven terrain under various ground conditions such as asphalt, gravel, mud, or grass. The platform consists of two chassis parts, the front part housing the motor and the hydraulic block, and the rear part incorporating the forks attached to the lifting mast. The motor side is designated as the main driving direction for autonomous operation, see Figure 4. This is motivated by considerations of load handling safety and operational visibility due to the unobscured view.

ADAPT has been extensively customized for automation since 2019 as part of several funded national and international research projects. Figure 3 illustrates the current hardware setup, highlighting the added components required for autonomous operation. The following sections provide a detailed overview of the hardware architecture and emphasize the differences between the automated prototype and the platform for manual operation.

#### 3.2. Actuation

As shown in Table 1, the BM154 platform uses a diesel engine as its main power source, driving two distinct hydraulic circuits that control vehicle movement and operational functions. The diesel engine drives a closed hydraulic

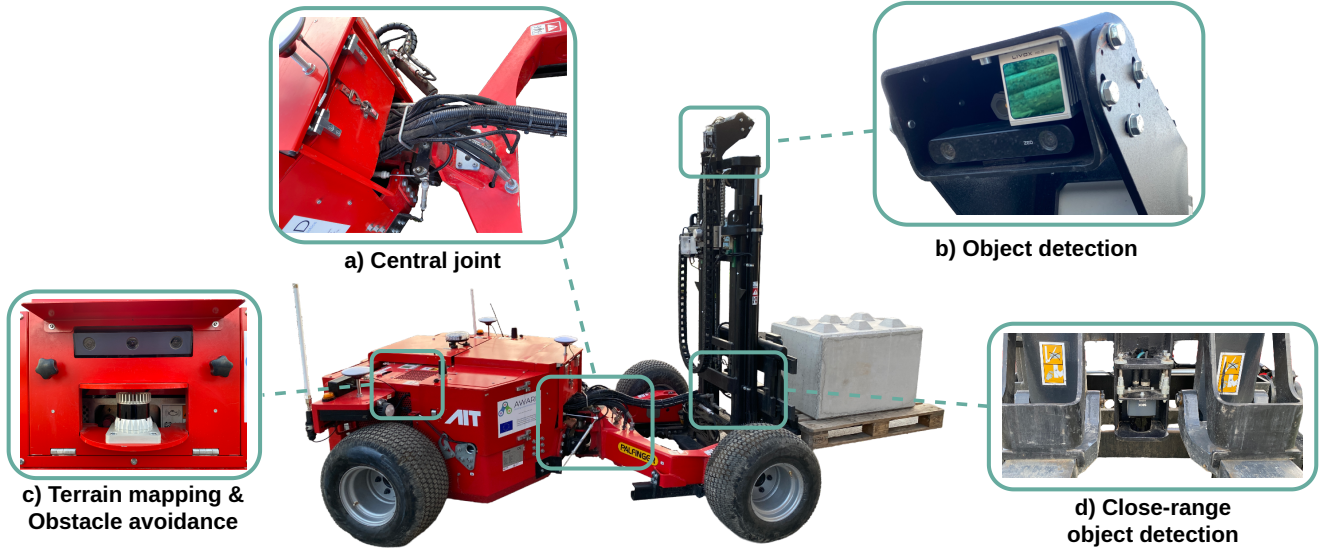


Figure 3: Key hardware components of ADAPT. (a) 3D Central joint for maneuverability and structural flexibility, (b) Object detection system, (c) Obstacle avoidance and terrain mapping sensor, and (d) Close-range object detection for precise load handling.

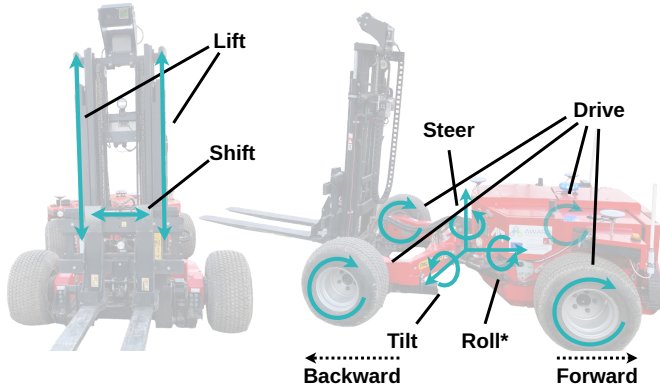


Figure 4: Actuated and unactuated(\*) joints for vehicle base movement and fork positioning.

circuit designed for operating the wheels, as well as an open hydraulic circuit responsible for actuating multiple hydraulic cylinders, amongst others for steering and lifting the forks. Figure 4 and Table 2 provide graphical and concise textual information on the forklift's actuated and non-actuated joints, driven by the hydraulic motor and cylinders.

The closed hydraulic circuit is tasked with driving the vehicle's wheels, delivering continuous hydraulic traction to ensure efficient power transfer and enhanced mobility. This design optimizes vehicle stability and maneuverability, particularly in challenging or uneven terrains. The hydrostatic four-wheel drive system is controlled by a PWM signal, where the duty cycle determines the flow rate of the hydraulic fluid, which in turn directly governs the wheel speed.

The open system discharges hydraulic fluid after use into the tank, making it more suitable for functions that require intermittent actuation. The open circuit governs

several essential functions, including steering and tilting of the central joint that connects the front and rear chassis (see Figure 3a). Although the rolling rotation of the chassis is passive and not directly actuated, it is fundamental to maintaining ground contact and load distribution on irregular terrain. The open circuit also facilitates mast actuation, allowing vertical fork movement (lifting and lowering) and lateral adjustments (shifting left and right). The control of the open hydraulic system's cylinders is facilitated by proportional valves, which allow precise control of valve spool positions via a CAN interface.

Table 2: Interfaces for actuation and proprioceptive feedback for joint position, velocity, and hydraulic pressure. ✓ indicates directly available interfaces, while ✗ denotes unavailable ones. ✓ signifies feedback that is obtained through post-processing of sensor data.

	Active Actuation	Position Feedback	Velocity Feedback	Pressure Feedback
<b>Drive</b>	✓	✗	✓	✓
<b>Steer</b>	✓	✓	✓	✓
<b>Tilt</b>	✓	✓	✓	✓
<b>Roll</b>	✗	✓	✓	✗
<b>Lift</b>	✓	✓	✓	✓
<b>Shift</b>	✓	✓	✓	✓

### 3.3. Sensing

This section describes the proprioceptive and exteroceptive sensing hardware components of ADAPT. Proprioceptive sensors monitor the vehicle's internal state, enabling precise joint control, while exteroceptive sensors facilitate accurate pallet and loading platform pose estimation, vehicle localization and mapping, and obstacle detection. Advanced algorithms that process sensor data and enable higher-level decision-making and motion control are discussed in Sections 4 and 5.

### 3.3.1. Proprioception

The forklift’s proprioception system integrates several sensors to monitor its internal state with high precision, especially the joint values depicted in Figure 4. In terms of vehicle motion feedback, wheel speed encoders are used to monitor the rotational velocity of each wheel. To capture the 3D rotation of the central articulated joint, a system utilizing three linear potentiometers was designed. By measuring the sensor elongation, the three articulation angles can be calculated with sub-degree precision. The resulting values are integral for steering the vehicle and precisely adjusting the fork tilt angle during load manipulation. Pressure sensors are installed within the hydraulic cylinders and the hydraulic drive system to measure pressure levels at high frequency. These measurements are crucial for controlling the forklift’s load-handling capabilities, including detecting whether the fork is in direct contact with the environment. In addition, draw-wire encoders are implemented to measure the vertical position of the lifting mast and the lateral movement of the forks (side-shift) with millimeter precision. Together, these sensors provide comprehensive real-time feedback and allow for accurate modeling of the behavior of the system.

### 3.3.2. Exteroception

In robotics, the exteroceptive system refers to the sensors and mechanisms that allow a robot to perceive and interpret information from its environment. For ADAPT, the exteroceptive system is crucial for localization and mapping, precise object detection, traversability assessment, and obstacle avoidance, ensuring safe and efficient operations in complex environments. The sensor placement on the machine is chosen according to their function and the phase of operations they are required in, see Figure 3. High-resolution 3D mapping of the environment and obstacle detection is performed by the wide field of view Ouster OS1-64 LiDAR, mounted in the machine’s forward direction, see Figure 3c. In fork/backward direction, a narrow field of view Livox Mid-70 LiDAR sensor, and a ZED2i stereo camera are employed for object detection, see Figure 3b. In the forward direction, the system moves faster and covers longer distances, increasing the risk of collisions with dynamic obstacles. Thus, active low-latency obstacle detection is crucial during path execution. In the backward direction, where pallets are only loaded and unloaded, explicit obstacle detection (going beyond terrain mapping) is not essential.

For pallet recognition, the ZED2i is the central component. It provides the input data for the neural networks for pallet recognition and pose estimation. Additionally, for precise short-range detection during the final pallet approach, the forklift is equipped with a Sick picoScan150 2D LiDAR, Figure. 3d. It ensures accurate positioning of the forks relative to the pallet, due to its high frequent update rate and well-aligned viewing angle. To enable accurate detection of the truck’s loading edge, the forklift utilizes the Livox LiDAR. Additionally, a Septentrio mosaic-H system

with two antennas is used for RTK GNSS localization. It provides accurate position information at the centimeter level and heading information to ensure precise alignment during loading and unloading tasks.

By integrating these sensors, the exteroceptive system equips ADAPT with comprehensive situational awareness, supporting centimeter-accurate load handling and safe navigation in outdoor settings.

### 3.4. Processing Components and Network

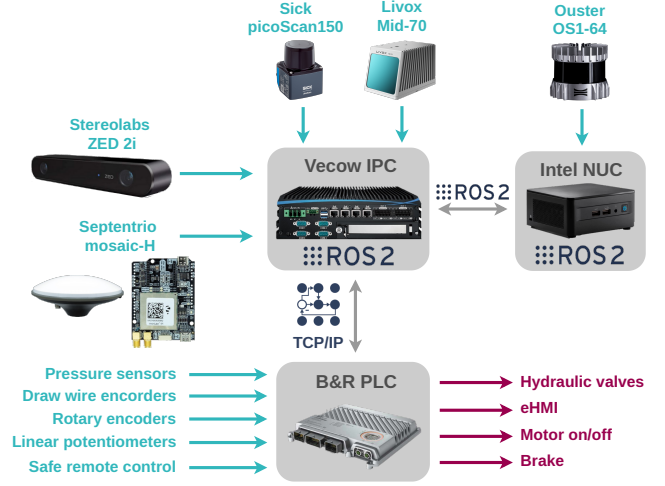


Figure 5: Overview of the main hardware components, including core processing devices, actuators, as well as proprioceptive and exteroceptive sensors.

ADAPT is designed with a robust and distributed processing hardware architecture, depicted in Figure 5. The core system consists of three primary computational components: a Programmable Logic Controller (PLC), a rugged industrial PC (IPC), and an additional compact, high-performance PC (NUC), each assigned distinct responsibilities.

The B&R X90 PLC is dedicated to managing low-level hardware interfaces, including direct connections to sensors and actuators that require low latency and real-time control. It also handles safety-critical operations that depend on rapid response times, such as emergency stops. The rugged IP67-compliant design of the PLC makes it suitable for harsh outdoor environments and does not require an additional enclosure. For higher-level processing, such as planning, advanced control algorithms, and managing intelligent sensors, a Vecow 1210 IPC is employed. It connects to the PLC via a central Ethernet switch to receive the low-level sensor data and to transmit high-level commands over a custom TCP/IP protocol. This setup enables seamless integration and coordination between low-level operations and advanced computational tasks that do not require millisecond-level latency. These advanced computational tasks include high-level task and motion control, vehicle state estimation, and object detection pipelines, utilizing camera and LiDAR sensors. The NUC unit is responsible

for processing data from the Ouster LiDAR, allowing both mapping the vehicle’s environment and obstacle avoidance and sharing the respective data via the Robot Operating System (ROS 2) [65] over Ethernet.

A wireless network bridge connects the forklift to a remote monitoring station housed in a weatherproof container, primarily supporting development and expert interventions. This setup enables live monitoring of the system’s operation, ensuring efficient debugging and adjustments during testing phases. Additionally, a supplementary WLAN antenna provides on-site operators with the ability to monitor the system state via a tablet-based Human-Machine Interface (HMI). For long-range communication, an LTE/5G router is integrated.

All components discussed, along with the necessary power supply electronics, are IP67 rated or housed within weatherproof switching cabinets, ensuring reliable operation under all typical weather conditions in Central Europe.

### 3.5. Software Components

Figure 2 shows an overview of the software architecture as well as concise descriptions of core functionalities and their associated hardware components. Core functionalities include localization and mapping, object detection, obstacle detection, task planning, and motion control. Localization and mapping are based on GNSS modules and LiDAR to provide accurate environmental maps and vehicle positioning data. Object detection utilizes a stereo camera as well as LiDAR to identify pallets and truck loading edges, facilitating precise load carrier handling. The obstacle detection module ensures safety by halting the vehicle before potential collisions with detected obstacles. The task planner serves as the central planning component of the system, managing high-level decision-making and coordinating both the path planner and motion controller. The path planner creates optimal routes based on map and localization data, while the cascaded motion controller provides precise vehicle base movements and responsive fork actuation for effective pallet manipulation. The majority of the software components running on the rugged IPC and the NUC highly depend on the ROS 2 middleware and its associated libraries, which enable a decentralized architecture while ensuring robust data and information exchange. A detailed discussion of the modules presented can be found in Sections 4 and 5.

## 4. Perception

ADAPT relies on multiple perception modules to function effectively in an outdoor environment. The first requirement is self-localization within its surroundings, which is integrated with mapping of pallet poses in a simultaneous localization and pallet mapping process; see Section 4.1. However, a more detailed environment mapping is necessary to assess terrain traversability, as shown in Section 4.2.

Since autonomous exploration on a public construction site is infeasible, we assume an initial human-guided exploration phase. A human controller then designates general loading and unloading areas to define the mission: which pallets should be brought where, and how many. Within these areas, ADAPT autonomously detects all pallets and trucks and estimates their 6D poses. The pallet detection process is described in Section 4.3, while the estimation of the edge of loading of the truck is covered in Section 4.4. Lastly, to ensure safe navigation and prevent collisions during path execution, the forklift must detect and take into account obstacles in its surroundings, as discussed in Section 4.5.

### 4.1. Joint Localization and Pallet Mapping

The goal of mapping is to derive a representation of the environment that is as rich in features as necessary for the application, but as compact as possible to keep computational complexity low. For ADAPT, there are two levels of abstraction in which we need to map the environment in: The high-level representation of the pallet poses, and the lower-level environment map with a strong focus on terrain traversability assessment, see Section 4.2.

For high-level joint location and pallet mapping, we use a factor graph-based approach [66] that allows the integration of vehicle odometry data, GNSS measurements and pallet detections in a joint optimization framework. A factor graph is a theoretical framework that models unknown variables, measurements, and their interdependencies as a bipartite graph with two types of nodes, see Figure 6. It consists of variable nodes (depicted as circles), which represent the variables to be estimated, and factor nodes (depicted as rectangles). In this context, factors can be binary (functions that relate two unknowns with one another) or unary (constraints on a variable based on a measurement). This factor graph approach is advantageous in this context as it allows flexible integration of multiple types of measurement and provides a probabilistic framework for managing uncertainties inherent in noisy and delayed sensor data. Our factor graph is shown in Figure 6. We use GNSS measurements from a dual antenna system that provides global position and attitude information. The forklift pose nodes are connected using odometry which is based on wheel encoders and steering angle measurements. Pallets are detected and their poses are estimated from different viewpoints and forklift poses, respectively. Therefore, the estimation of the pose of the pallet is represented as a binary factor linking the position of the pallet with the location of the vehicle. To maintain real-time performance, we build upon iSAM2 [33] incremental smoothing, which yields the jointly most probable pallet and forklift poses given all odometry, GNSS, and pallet measurements. This allows the pose of a pallet to be optimized by measurements from different views. In addition, the pallet poses and vehicle location are optimized even without or with a less precise GNSS signal.



With iSAM2 updates of pallet detections and localization information are optimized incrementally, in contrast to re-solving the entire optimization repeatedly. To do so, iSAM2 maintains, in addition to the factor graph, a dynamic Bayesian tree structure to track variable inter-dependencies. This approach ensures that updates to the factor graph are confined to regions where changes in inter-dependencies occur. To facilitate real-time operation, our iSAM2-based optimization approach for joint pallet and vehicle pose mapping

- linearizes the problem around an initial guess,
- reinitializes (recomputes the linearization) when a variable changes significantly,
- exploits the sparsity of the optimization problem, since each factor connects only a small subset of variables, leading to a sparse Jacobian matrix,
- simplifies (marginalizes the optimization problem) by pruning redundant vehicle and pallet poses to facilitate long-term operation,
- performs pose pruning and culling for measurements older than a certain time (currently set to 5 seconds) to keep the measurement history maintainable.

This approach can efficiently integrate information from odometry sensors, GNSS, and detections over time in a way that yields, given all sensor information, the most probable result for the unknowns (the maximum a posteriori estimate). The pallet mapping is tightly integrated into our optimization framework. For pallet tracking, we use a Mahalanobis distance-based [67] approach to ensure a robust association of detections between consecutive measurements. The Mahalanobis distance metric allows for dynamic association by accounting for both positional variance and estimated noise in pallet positions. Additionally, pallets are dynamically managed within the forklift’s view frustum by pallet bookkeeping that goes beyond pure variable marginalization (pruning). It manages the tracking of new never-before-seen pallets, associates new detections with old ones, and deletes pallets if they should be in sensor view but cannot be detected for a while. This approach aligns with the concept of object permanence, where pallets are presumed to remain at a designated location even when they are not directly visible.

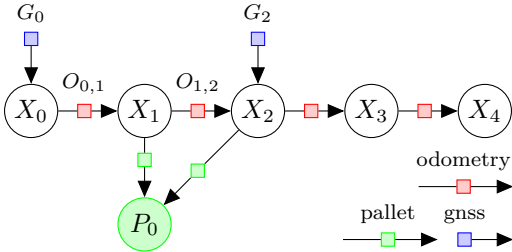


Figure 6: Factor Graph for the joint forklift poses ( $X_x$ ) and pallet poses ( $P_p$ ) over time (left to right), relative (from one time step to the next) odometry information  $O_{p1,p2}$ , and GNSS measurements  $G_g$ . In this example, the pallet  $P_0$  has been detected in timestep 1 and 2, in timestep 0 and 2 GNSS information was available.

#### 4.2. Traversability Mapping

The targeted area of application, e.g., construction sites, of ADAPT are unstructured environments with potentially uneven terrain. Hence, a specific environment mapping targeting these aspects is required. Therefore, a 2.5D elevation map representation is generated from the 3D point measurements of the Ouster LiDAR. While path planning complexity can be reduced to planning in 2 dimensions, the most relevant geometric information about the environment must still be available from the map. In particular, it must allow for a clear distinction between traversable areas, obstacles, and slopes. This distinction is crucial for forklifts, as they are more susceptible to tipping over when carrying loads.

Similarly to *spatial-temporal voxel layers* [20], our approach aggregates data into a 3D voxel grid with short-term memory. However, instead of directly deriving a 2D costmap, our method employs a 2.5D elevation map for dynamic obstacle handling and terrain analysis, serving as a long-term memory representation. Therefore, it is implemented as a three-stage process, encompassing the analysis of single scans, 3D voxel map aggregation, and the generation of a 2.5D elevation map. In all three steps, distinguishing between ground points and obstacle points plays a decisive role.

**Analysis of Single Scans:** Single scans are analyzed within the sensor domain, utilizing the unique capabilities and characteristics of the sensor. By focusing on individual scans, this stage minimizes disturbances caused by alignment errors. Parameters such as the height above ground and the angle between the surface normal vector and the vertical axis help determine the probability of a point being an obstacle. For the Ouster LiDAR, a single swipe of the nearly  $180^\circ$  field of view that is used constitutes a scan. The ego-motion during this rotation is compensated by transforming all points into the sensor’s coordinate system at a fixed timestamp.

**3D Voxel Map Aggregation:** The second stage involves short-term aggregation of single-scan point clouds into a 3D voxel map, which can be performed based on time intervals or distance traveled. This process improves point density and addresses gaps caused by the LiDAR’s sampling patterns. Additionally, statistical methods are used to remove outliers. Overhanging structures, which present challenges for elevation maps, are identified by analyzing the free space between the ground and these structures. The resulting output is an update for the elevation map, where each cell in the horizontal plane contains a computed elevation value and obstacle probability derived from the vertical voxel stack.

**2.5D Elevation Map:** The 2.5D elevation map integrates updates from the voxel map to form a long-term representation of the environment. Obstacle probabilities are compared, which may lead to confirmation and fusion of values or discrepancies. In the case of discrepancies, the classification of a cell can change from obstacle to floor, or



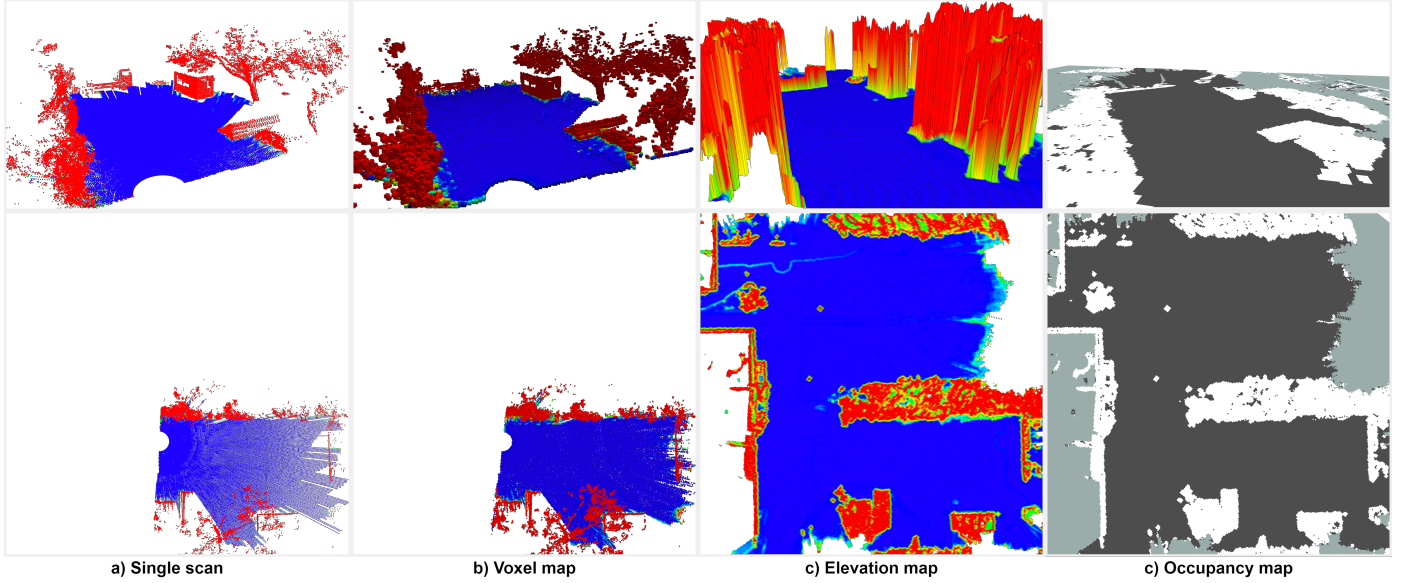


Figure 7: Mapping stages. Top row: 3D view. Bottom row: Top view. The color shows the traversability from blue (good) to red (bad).

vice versa. When a state change occurs, the affected cell is completely replaced with the new values. This approach allows the map to adapt to changes such as the appearance, disappearance, or movement of objects. Adaptability is crucial for robots, such as forklifts, that actively manipulate their environment. The final traversability analysis combines obstacle probabilities with slope information derived from the elevation map’s geometry. A tiling scheme ensures that the system can function in unbounded environments.

The final output of the mapping process is an occupancy map containing critical spatial information, which serves as a 2D input for collision-free path planning. Figure 7 shows example views of the mapping stages at our test site in the outdoor laboratory, where the evaluations in Section 6 were performed.

#### 4.3. Pallet Detection and Pose Estimation

Detecting pallets and accurately determining their 6D pose is essential to enable ADAPT to interact with them effectively. This is particularly important in construction sites, where, unlike in controlled environments such as warehouses, pallets are typically placed arbitrarily rather than following a fixed grid or placement schedule. The pallet detection methodology used is described in detail in [40]. Given a dense stereo depth image as input, we intend to detect and estimate the 6D pose of multiple pallet instances with known structure and dimensions in a scene. To derive and exploit a learned neural representation, we proceed as follows:

**Pallet representation:** Pallets are represented by a part-constellation model, see Figure 9a, where pallet corners and edges not only form a localized part, but at every pixel they also define a spatial vote offset attribute, implying the offset vector to the corresponding object center. Part locations and local vote vectors are learned from

synthetic data.

**Data generation:** A synthetic data generation pipeline is used where more than 150 thousand stereo image pairs are generated with diverse pallet configurations, e.g., orientations, items carried, clutter. The data generation step relies on a simulated stereo camera setup, matching the baseline and optics of a ZED2i stereo camera [68]. The synthetic stereo image pairs are used in a stereo depth computation step, which results in depth data exhibiting similar data characteristics as depth computed from real stereo pairs. This low sim-to-real gap allows for generating a rich variety of view variations and pallet configurations for learning.

**Learning:** We employ an extensible convolutional encoder-decoder framework, based on [69], which estimates outputs for multiple learning tasks, see Figure 8. Pallets are represented by a part-based representation, where each part also carries a spatial vote offset attribute, where the offset vector points to the corresponding object center. During training key-point and line segment representations yield multichannel heatmap output representations, where each channel is assigned to respective corner/edge categories.

**Detection and pose estimation during inference:** During inference, we use the stereo depth input of the ZED2i on-board camera to detect part-instances of pallet objects, where inferred parts are used to vote for pallet centers in a probabilistic manner, orange arrows in Figure 9a. Careful analysis of extensive key-point-based pose estimation experiments has revealed that detected points located on the approach side are more accurately determined than those farther away from the sensor. To mitigate the effect of spatially uneven distribution of re-projection errors on pose estimation, we set the pallet’s origin to the center of the approach side, as illustrated in Figure 9b.

To obtain the final 6D pose relative to the sensor, we

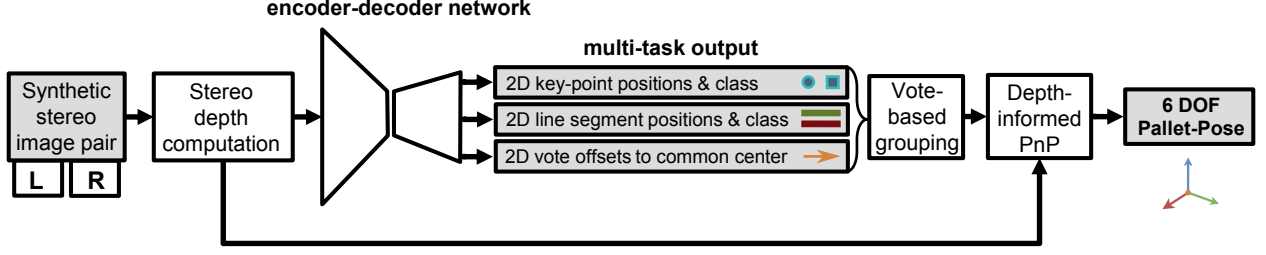


Figure 8: Overview of learning/inference pipeline estimating multiple 2D parts, which are used for 3D pose estimation, symbols in Figure 9.

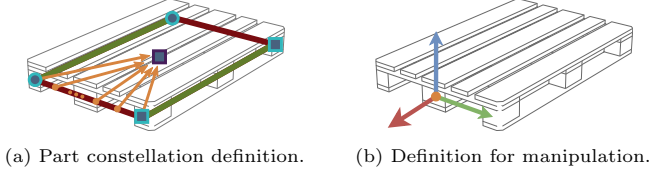


Figure 9: Different pallet representations: For machine learning (a), the pallet is composed of two corner types (circle/rectangle) and two line classes (red/green) voting (orange) for a pallet center. In contrast, for manipulation, the basis of the pallet is located at the center of the approach side, see labels in Figure 8.

integrate a perspective-n-point (PnP) formulation (see [70]), with available depth information, as a joint optimization problem. Depth information is only used on the approach side, as it is visible to the sensor.

Since pallets can exhibit slight dimensional deviations and corner detections are subject to uncertainties from the model, we applied a final refinement step. Specifically, we adjust the pallet position using stereo depth measurements from the front midpoint. This final correction step helps ensure a more accurate and stable pose estimate in real-world conditions.

**Pose estimation accuracy:** By analyzing the geometry of Euro-pallets and fork dimensions, precise tolerance values for pallet insertion can be established. Consequently, pose estimation errors serve as a key metric for evaluating the effectiveness of the proposed approach in achieving accurate insertion. The ground truth data for error computation was obtained through manual annotation of a point cloud captured by an extrinsically calibrated LiDAR sensor mounted adjacent to the camera. Figure 10 presents the evaluation results based on 170 detections, covering various load types at different distances and orientations. To compare a detection with its corresponding annotation, the estimated 6D pose was transformed into a coordinate system centered at the manually annotated pose, cf. Figure 9b, yielding a 6D error vector  $\mathbf{e} = [e_x, e_y, e_z, e_\phi, e_\theta, e_\psi]^T$ . The tolerance limits for the relevant degrees of freedom are  $y_{tol} = \pm 0.05m$  and  $z_{tol} = \pm 0.04m$ , with respect to the pallet coordinate system. The constraint in the x-direction is theoretically determined by the load's center of mass, however, complete fork insertion is preferable to ensure optimal transport stability. Assuming the pallets remain parallel to the ground, detections with unsuitable roll and pitch angles are filtered out, as the forklift cannot successfully

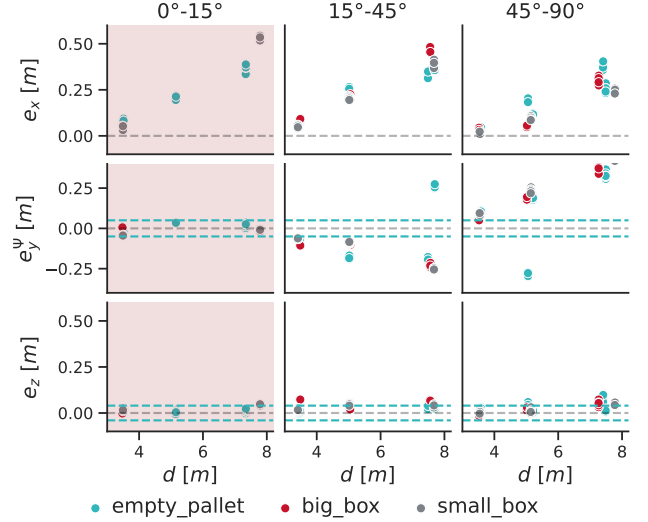


Figure 10: Pallet pose estimation errors over the distance to sensor  $d$  for various load types. Columns represent different orientations around the pallet's z-axis. Dashed lines indicate tolerance boundaries for successful fork insertion, with the highlighted  $0^\circ$ - $15^\circ$  range being critical for insertion.

pick them up. Thus, these dimensions are excluded from the evaluation. Errors in the y-direction  $e_y$  are affected by deviations in orientation around the pallet's z-axis, which modify the effective pallet opening by a factor of  $\cos(e_\psi)$ . To account for this influence, the corrected y-direction error is computed as  $e_y^\psi = \frac{e_y}{\cos(e_\psi)}$ .

The results indicate that detection accuracy deteriorates with increasing sensor distance, particularly in  $e_x$ , due to the quadratic increase in depth error inherent in stereo vision. Furthermore, when the pallet is rotated around its z-axis, the error distributes between  $e_x$  and  $e_y$ . Overall, the results suggest that a single detection at angles exceeding  $15^\circ$  is often insufficient for successful pallet loading. However, as the sensor approaches the pallet, the detection quality improves, maintaining errors within tolerance limits in most cases and enabling a successful interaction.

#### 4.4. Loading Edge Detection

To accurately position pallets on the truck, the system performs a LiDAR point cloud-based detection of the loading platform, once per load cycle. Given the transformation of the LiDAR sensor relative to a globally planar coordinate

frame and a set of 3D points aggregated from LiDAR point clouds over a period of time, the loading platform detector follows a multi-step procedure:

**Outlier Removal:** Outliers are removed by discarding points that lack a sufficient number of neighbors within a specified radius.

**Height Filtering:** The point cloud is refined to include only points within 0.2 and 2.5 meters above the ground.

**Edge Candidate Points Identification:** Points are classified as edge candidate points if their neighborhood contains two distinct sets of points with orthogonal normals. One normal direction must align closely with the vertical (up) vector, meaning that the other direction must be parallel to the ground plane.

**Edge Line Detection:** A RANSAC (Random Sample Consensus) approach is used to find a line that has strong support in terms of the number of candidate edge points.

**Loading Edge End Detection:** The vertical front-face of the loading platform is detected. The loading edge and the front surface together define a reference frame.

**Pallet Slot Definition:** A configurable loading pattern defines target slot placements, depicted in Figure 11.

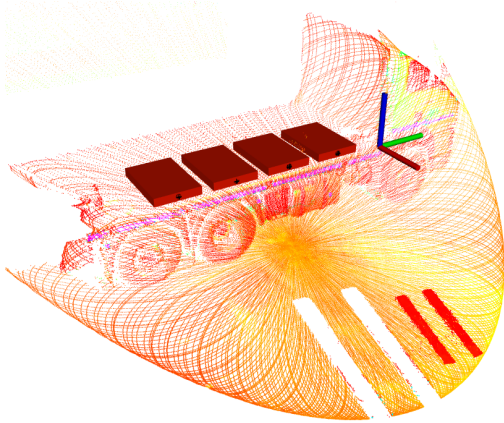


Figure 11: A LiDAR point cloud (colored by reflectance) captures the scene, including the forklift forks (bottom right). The lift is positioned at an estimated loading height to optimize the platform’s visibility. The resulting detected loading edge reference frame (RGB frame) and the target slots (red boxes) defined within this frame are depicted as overlay.

This process ensures reliable detection of the loading platform, even under challenging conditions, which works regardless of the tilt of the truck or partial loading because it focuses solely on the edge. Additionally, an image segmentation method for part detection was tested [71], but turned out to be more prone to clutter on the platform than this geometry-specific deterministic edge detection.

#### 4.5. Obstacle Detection

For safe operation, the forklift must detect obstacles quickly to avoid collisions with both static obstacles (trees, walls, etc.) and moving obstacles (excavators, pedestrians, etc.) which may approach the currently planned drive path. The implemented approach is a fast-reacting method

in the sensor frame complementary to and independent of the mapping approach presented in Section 4.2. It is applied only in the forward driving direction, where the risk of colliding with moving obstacles is higher, whereas movements in fork direction, as discussed in Section 3.3.2, are slower and follow much shorter paths. Based on the selected safety concept, when an obstacle is detected, the forklift is brought to a safe state (standstill) to prevent collisions, rather than re-planning its path to navigate around the obstacle. Once an emergency stop is triggered, the forklift remains stationary until it receives operator input to resume the task.

For the assessment of the risk of collision with moving obstacles, we utilize a multi-object detection and tracking system, originally based on the works [72] and [73], which further became the basis for an endurance-tested tramway braking assistance system in commercial use<sup>2</sup>. It operates in a tracking-by-detection paradigm. It can detect arbitrary objects, track them over time, and assess if a collision will occur based on the predicted trajectories of the objects and the projected path of the forklift. The detection step is based on generic 3D clustering, hence it does not depend on predefined object classes such as person or vehicle.

To detect obstacles, the system analyzes point clouds from the Ouster LiDAR mounted on the front part of the forklift. Both LiDAR and a custom stereo camera setup, see Figure 3c, have been successfully used, but the wider field of view of the LiDAR system makes it the safer choice for obstacle detection, see Figure 12. Points above an assumed ground plane, cf. Figure 12a, are analyzed for potential obstacles by grouping them into separate distinct objects using Density-Based Spatial Clustering of Applications with Noise (DBSCAN) [74]. The clusters represent potential obstacles (indicated as red and green boxes in Figure 12) but only if they overlap with the expected vehicle’s path and are considered potential collision objects (red) that trigger an emergency brake. The volume of the monitored path, cyan in Figure 12, is defined by extruding the vehicle footprint (plus an additional clearance buffer) along a simplified vehicle path. Obstacle bookkeeping is implemented in a manner similar to pallet bookkeeping, as described in Section 4.1. However, it is enhanced with a Kalman filter based on a constant velocity model to accommodate movement. Then each object track is checked for a possible collision, which can cause a collision warning based on the predicted movement of the object, the velocity of the forklift, the characteristics of the forklift deceleration, and a defined minimum safety distance.

## 5. Planning and Control

ADAPT performs two primary types of actions to carry out its tasks effectively: (1) collision-free *Navigation*, where

<sup>2</sup><https://www.alstom.com/solutions/rolling-stock/citadis-light-rail-designed-reflect-your-citys-unique-identity> (accessed 2024-12-11)



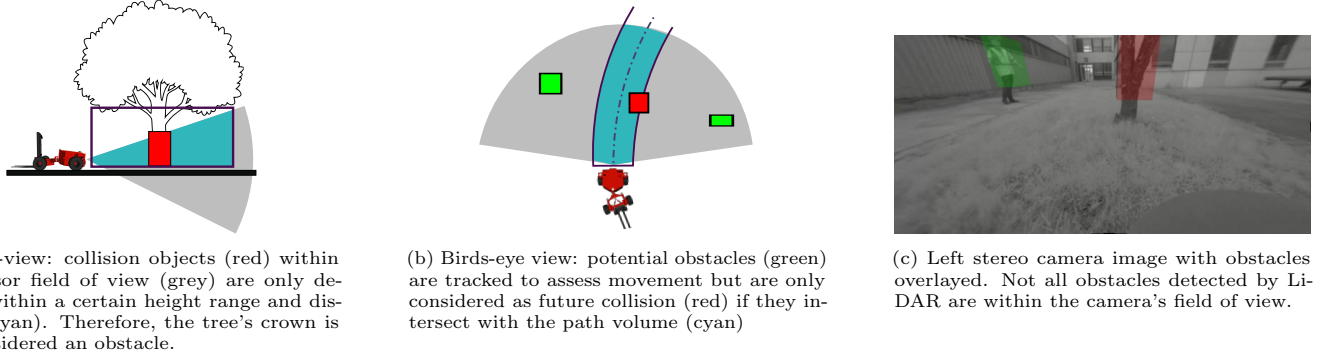


Figure 12: Depiction of the obstacle detection system's geometric relations and output. Definitive collision objects (red) that trigger emergency braking overlap with the expected path volume (cyan) and tracked potential obstacles are outside (green).

the forklift moves from its current position to a target location within a predefined operational area, either while carrying a pallet or traveling unloaded, and (2) precise *Manipulation*, which involves the accurate pickup and placement of pallets in specified locations (slots), such as on a truck or within a designated area on the ground (multiple slots on a truck are shown in Figure 11).

This section explains how these actions are coordinated throughout the operational workflow and the measures implemented to ensure their accurate and reliable execution.

### 5.1. Task planning and Execution

Task (re-)planning and execution are crucial for the efficient operation of autonomous machines, particularly in dynamic, unstructured environments, enabling them to adapt to changing conditions. In the proposed automated system, task planning and execution are achieved using a behavior tree-based approach. Behavior trees provide a flexible, modular framework for modeling decision-making processes and task execution in a hierarchical, reactive manner [75]. A behavior tree consists of action nodes (which perform tasks), condition nodes (which evaluate specific states), and composite nodes (which control the flow of execution, such as sequences and fallbacks). This structure allows for scalable and adaptable behavior design, making it particularly suited for managing complex tasks like navigation and object manipulation. The integrated behavior tree logic is based on the BehaviorTree.CPP library [76], which offers a performant set of tools for behavior tree construction and execution. To enable smooth communication with the robot's ROS 2 based architecture, the ROS 2 wrappers from the Nav2 framework [77] are utilized. A simplified version of the behavior tree that describes the operation of ADAPT is shown in Figure 13. The flow of execution can be summarized as follows:

1. The sequence begins with ADAPT searching for pallets using the *FindPallets* action.
2. Once pallets are identified, the *SelectPallet* action determines which pallet to target based on predefined criteria.

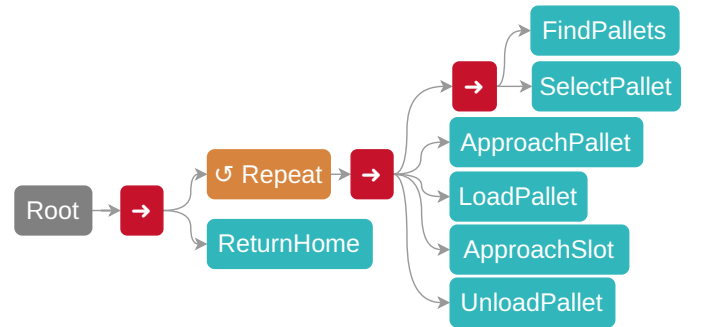


Figure 13: Simplified behavior tree for the proposed system, consisting of the root node (gray), action nodes (cyan), sequences (red) and a decorator node (orange).

3. The *ApproachPallet* action guides ADAPT to navigate toward the selected pallet.
4. Once positioned correctly, the *LoadPallet* action ensures the pallet is securely lifted onto ADAPT.
5. ADAPT executes the *ApproachSlot* action to navigate to the designated slot or unloading area.
6. At the slot, the *UnloadPallet* action places the pallet in its target location.
7. After completing the unloading task, the behavior tree loops back using the *Repeat* element and is ready for the next pallet. After loading all pallets, the *ReturnHome* action navigates ADAPT to its home position.

The full behavior tree is significantly more complex, featuring 26 custom sub-trees and over 30 unique action and composite nodes. It integrates both reactive and anticipatory behaviors. For example, a reactive behavior occurs after a failed pallet pick-up attempt, due to *e.g.*, inaccuracies in the estimated pose, triggering a recovery action and another pick-up attempt.

To initiate the operation, *i.e.* the execution of the behavior tree, ADAPT receives a command by the forklift supervisor to transport either a specified number of pallets or all available pallets from a designated loading zone to an unloading zone. The current system iteration features a tablet-based HMI for monitoring and controlling the ve-

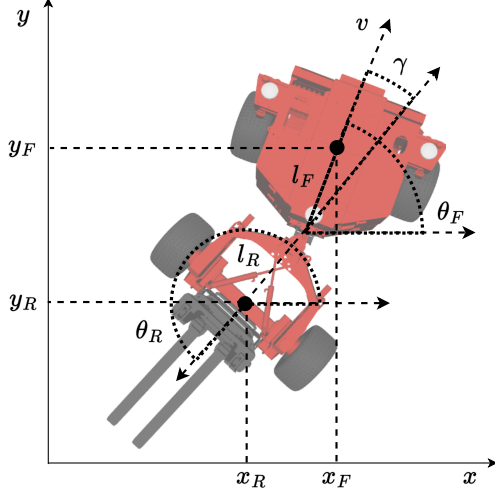


Figure 14: Articulated forklift kinematics with the front part  $\mathbf{q}_F = [x_F, y_F, \theta_F]^T$ , where  $x_F$  and  $y_F$  represent the position in the 2D plane, and  $\theta_F$  its orientation. The rear part is characterized by its own position and orientation  $\mathbf{q}_R = [x_R, y_R, \theta_R]^T$ . The angle of the articulated steering joint is denoted by  $\gamma$ .

hicle's operation. The framework also supports testing of novel interaction modalities, like gesture control, freeing the hands of an operator, see [78] for details.

## 5.2. System Models

Accurate modeling of the vehicle's kinematics and hydraulic actuators allows precise motion control. This is essential for efficient operation in complex environments, allowing for reliable navigation and pallet manipulation.

### 5.2.1. Vehicle Base Kinematics

The two parts of the vehicle chassis are connected by an articulated joint as described in Section 3.2. This allows modeling the movement on the 2D plane using articulated vehicle kinematics, as shown in Figure 14, as

$$\begin{bmatrix} \dot{x}_F \\ \dot{y}_F \\ \dot{\theta}_F \end{bmatrix} = \begin{bmatrix} \cos(\theta_F) & 0 \\ \sin(\theta_F) & 0 \\ \frac{\sin(\gamma)}{l_F \cos(\gamma) + l_R} & \frac{l_R}{l_F \cos(\gamma) + l_R} \end{bmatrix} \begin{bmatrix} v \\ \dot{\gamma} \end{bmatrix}, \quad (1)$$

where the Cartesian coordinates of the front axle are defined as  $[x_F, y_F]$ , with its orientation represented by the angle  $\theta_F$ . The rear part  $\mathbf{q}_R = [x_R, y_R, \theta_R]^T$  is connected to the front part at the articulation point, with its orientation defined by  $\theta_R = \pi + \theta_F - \gamma$ . The kinematics are characterized by the system inputs  $v$  and  $\dot{\gamma}$  which are the velocity at the front axle and the steering rate, respectively. The parameters  $l_F$  and  $l_R$  are the center-to-axle distances from the front as well as the rear axle to the articulation point.

These kinematic equations, which model the motion of the vehicle in the 2D plane, are essential for path planning and vehicle base motion control. Extending this model to account for motion in 3D for steep terrain is an ongoing area of research and a focus of future work.

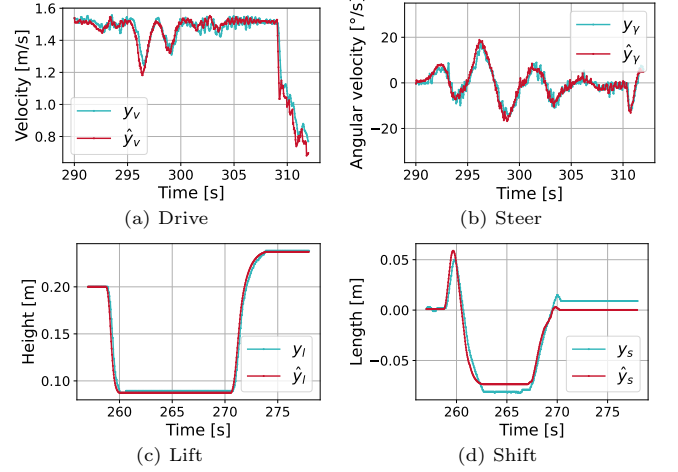


Figure 15: Results for modeling the hydraulic drive as well as the hydraulic cylinders showing the measured system output  $y_i$  compared to the estimated system output  $\hat{y}_i$ , calculated from the actuation command with  $i \in \{v, \gamma, l, s\}$ . (a)-(b) show data from a path following scenario, where as (c)-(d) show a pallet pickup maneuver.

### 5.2.2. Hydraulic Modeling

The flow rate of the hydraulic fluid in the hydrostatic four-wheel drive system is determined by the duty cycle of a PWM signal  $u_v$ , which has a nearly linear relation to the wheel velocity  $y_v$ . This is modeled by

$$\hat{y}_v(t) = K_1 \cdot u_v(t) + K_0, \quad (2)$$

with the estimated velocity  $\hat{y}_v$ . The parameterization of the constants  $K_0$  and  $K_1$  was empirically determined by identification runs. Figure 15a shows the estimated velocity  $\hat{y}_v$  compared to the measurement  $y_v$ .

The remaining degrees of freedom, namely steering( $\gamma$ ), tilting( $\beta$ ), lifting( $l$ ), and shifting( $s$ ), are actuated by hydraulic cylinders. The angular velocity of the steering joint  $\dot{\gamma}$  can be modeled as a linear function of the desired valve spool position of the steering cylinder  $u_\gamma$ , similar to (2). The other cylinders are modeled as first-order lag elements

$$\tau_\zeta \cdot \dot{\hat{y}}_\zeta(t) + \hat{y}_\zeta(t) = K_\zeta \cdot u_\zeta(t), \quad (3)$$

where the input  $u_\zeta$  represents the desired valve spool position for the corresponding actuated cylinder and  $\hat{y}_\zeta$  denotes the estimated output of the system,  $K_\zeta$  a model constant and  $\tau_\zeta$  a time constant for the model of  $\zeta \in \{\beta, l, s\}$  tilting, lifting and shifting, respectively. The results of the parameter identification experiments are shown in Figure 15, applied to a path following (Figure 15b) as well as a pallet pickup scenario (Figure 15c-15d). The estimated cylinder motion, denoted as  $\hat{y}_\zeta$ , aligns closely with the measured variable  $y_\zeta$ . However, when multiple cylinders are actuated simultaneously, the model's accuracy decreases due to altered pressure distribution and flow division, as well as pump limitations, leading to non-linear behavior. This reduction in accuracy is not significant in operation, as it can be compensated for by the feedback control system, discussed in the next section.



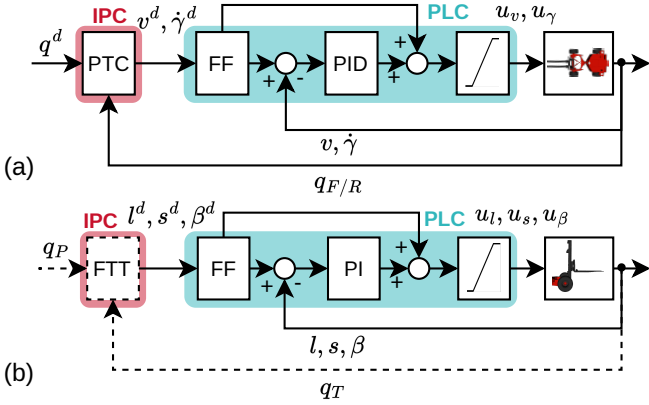


Figure 16: Cascaded control architectures for the vehicle base (a) and fork actuation (b), forming the foundation for pose-to-pose navigation and pallet manipulation. Main components, enclosed in red boxes, are the pose tracking control (PTC) and fork tip transformation (FTT) and run on the IPC, while those in cyan boxes operate on the real-time PLC. For navigation, FTT is not needed.

### 5.3. Motion Planning and Control

The operation of ADAPT is divided into two primary action types: (1) *Navigation* between poses, comprising path planning and following, and (2) *Manipulation* for loading or unloading of pallets. These primary actions share common vehicle functions, namely vehicle base and fork positioning control. These functions are implemented as two separate cascaded control structures, as illustrated in Figure 16. The main components of these control loops are the pose tracking control (PTC) and fork tip transformation (FTT) which track the external reference. The inner control loop consists of a feed-forward control (FF) based on the hydraulic models from Section 5.2.2 as well as basic PI(D) control and saturation blocks for hydraulic valve and cylinder control. This section delves into the details of the primary action types and explains how vehicle functions are implemented.

#### 5.3.1. Cascaded control

**Vehicle base control:** The algorithm to control the movement of the vehicle base is based on the kinematics of the articulated vehicle described in Section 5.2.1. It is inspired by the work presented in [59], which introduces a path-following strategy for articulated drum rollers that navigate straight paths through construction sites. The core concept involves tracking a virtual reference vehicle with coordinates  $\mathbf{q}^d = [x^d, y^d, \theta^d]^T$ , which serve as input of the Pose Tracking Control (PTC) component in Figure 16a. The reference pose  $\mathbf{q}^d$  can either represent a pose on a precomputed path or a pallet being approached. The exact methods for determining  $\mathbf{q}^d$  will be explained in the following sections.

The tracking is implemented by minimizing the state

of the error system

$$\begin{bmatrix} e_x \\ e_y \\ e_\theta \end{bmatrix} = \begin{bmatrix} \cos(\theta^d) & \sin(\theta^d) & 0 \\ -\sin(\theta^d) & \cos(\theta^d) & 0 \\ 0 & 0 & 1 \end{bmatrix} \begin{bmatrix} x_{F/R} - x^d \\ y_{F/R} - y^d \\ \theta_{F/R} - \theta^d \end{bmatrix}, \quad (4)$$

which is calculated by transforming the Cartesian coordinates of the reference vehicle into the vehicle's body-fixed origin  $\mathbf{q}_{F/R} = [x_{F/R}, y_{F/R}, \theta_{F/R}]^T$ . This can either be the center of the front (F) or the rear (R) axle. The state comprises the relative errors in longitudinal direction  $e_x$ , lateral direction  $e_y$  and of the heading  $e_\theta$ . The approach neglects  $e_x$  and instead focuses on minimizing  $e_y$  and  $e_\theta$  which results in the control law for the steering rate

$$\dot{\gamma}^d = -\frac{K_1 v(l_F + l_R)}{l_R} e_y - \frac{K_2(l_F + l_R)}{l_R} e_\theta - \frac{v}{l_R} \gamma, \quad (5)$$

derived using Lyapunov theory, as detailed in [59].  $K_1$  and  $K_2$  are control gains and determine the influence of the respective lateral and heading errors on the desired steering rate. The second input to the kinematic system is the desired forward velocity

$$v^d = \max(v_R - k_v(\dot{\gamma}^d)^2, v_{\min}), \quad (6)$$

which is designed to respect the constrained system's steering dynamics. In here,  $v_R$  is the desired reference velocity for operation. The parameter  $k_v$  allows to reduce the velocity proportional to the squared desired steering rate. Thus, sharp curvatures are tracked with lower speed, to maintain tracking accuracy. The minimum velocity  $v_{\min}$  ensures that the vehicle maintains a minimum speed, even during sharp steering maneuvers. Equations (4)-(6) build the foundation of the PTC and, thus, the cascaded control loop in Figure 16a.

**Fork positioning control:** For a successful pallet manipulation, an accurate positioning of the fork tip is necessary. The most critical is pallet pickup, where the tolerated positioning error must not exceed 5 cm. To this end, the tip of the fork  $\mathbf{q}_T = [x_T, y_T, \theta_T, z_T]^T$  must be precisely aligned with the pallet front  $\mathbf{q}_P = [x_P, y_P, \theta_P, z_P]^T$ , see Figure 19b. This is ensured by the fork tip transformation (FTT) component, as part of the cascaded control loop depicted in Figure 16b. The FTT transforms the target pose into the fork tip coordinate frame by

$$\begin{bmatrix} x'_P \\ y'_P \end{bmatrix} = \begin{bmatrix} \cos(e_\theta) & -\sin(e_\theta) \\ \sin(e_\theta) & \cos(e_\theta) \end{bmatrix} \begin{bmatrix} x_P - x_T \\ y_P - y_T \end{bmatrix}, \quad (7)$$

where  $e_\theta = \theta_P - \theta_T$ .

Based on (7), the reference signal for the fork shift corresponds to the lateral error,  $s^d = y'_P$ , and the lift mast height to the vertical error,  $l^d = z_P$ . The tilting command  $\beta^d$  is adjusted to keep the forks parallel to the ground. The cascaded loop in Figure 16b can operate without the FTT, depending on the forklift's current task. Specifically, during transporting a pallet - while not loading

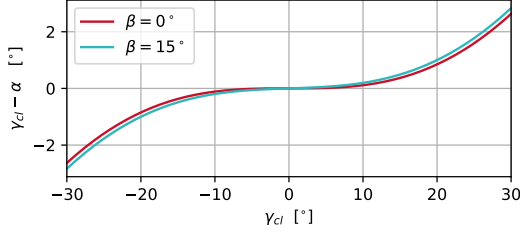


Figure 17: Deviation between car-like steering angle  $\gamma_{cl}$  and the articulation angle  $\alpha$ .

or unloading - the FTT becomes optional, allowing the setpoints for the underlying control loop  $l^d, s^d$  and  $\beta^d$  to be directly assigned to a transport position that keeps the fork at a safe height and angle.

### 5.3.2. Navigation

The *Navigation* action comprises the planning and subsequent following of a collision free path from one pose to another. Planning a path is a well-established research area for robotic applications, with numerous feasible algorithms. Empirical evaluation of potential path planners led to the conclusion that the Hybrid A\* stands out as particularly advantageous for flexible path planning in construction environments. This is due to its ability to plan near-optimal bi-directional paths while maintaining computational efficiency, and it places no restrictions on path length or the number and location of changes of driving direction. Additionally, the preferred driving direction can be forced with an adjustable penalty term.

However, the Hybrid A\* algorithm is formulated for car-like vehicles and cannot be directly applied to articulated vehicles. Nonetheless, for symmetrical articulated vehicles, *i.e.*  $l_R = l_F$ , the kinematic properties for static curvature and straight-line driving are equal to those of car-like vehicles. This is achieved by superimposing the Instantaneous Centre of Rotation (ICR), *i.e.* the intersection point of the front and rear axles, of both vehicle models.

Geometric transformations relate the steering angle of the articulated vehicle

$$\gamma = \arctan \left( \sin \left( \frac{\gamma_{cl}}{2} \right) \sqrt{2 (\cos(\alpha) \cos(\beta) + 1)} \right) \quad (8)$$

to the steering angle of the car-like model  $\gamma_{cl}$ . The relation between steering angle and articulation angle  $\alpha$  follows from the rotation between the front and rear part

$$\gamma = \arccos \left( \sqrt{\frac{\sin^2(\alpha) (\sin^2(\beta) - 1)}{2 (\cos(\alpha) \cos(\beta) + 1)}} \right). \quad (9)$$

These two equations (8) and (9) can be solved numerically for the steering angle  $\gamma$  or the articulation angle  $\alpha$ . Figure 17 shows the deviation between the planned angle  $\gamma_{cl}$  for car-like steering and the kinematic-matching articulation angle  $\alpha$ .

The Hybrid A\* implementation used in this work was developed in C++ using ROS 2 and is described in detail

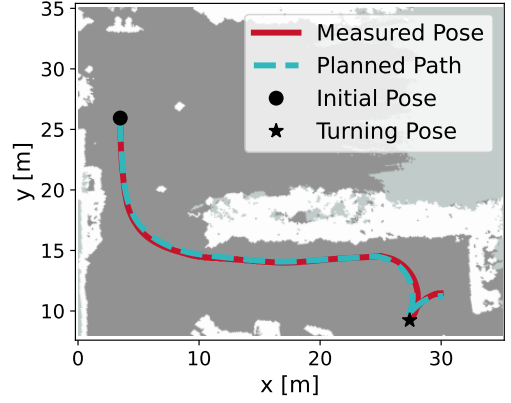


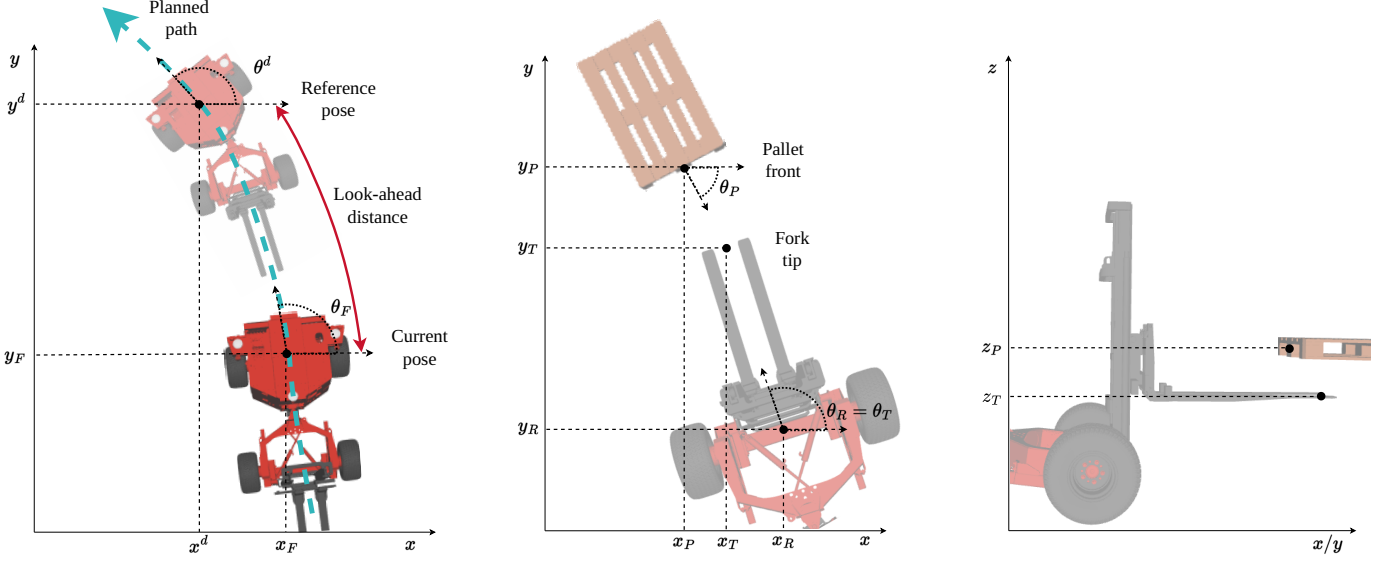
Figure 18: Bi-directional path planned (cyan), together with path tracking results (red) including one turning pose (★). White areas indicate obstacles.

in [79]. Figure 18 illustrates an exemplary path planning result for bi-directional movement. The occupancy map utilized for collision-free planning is generated using the algorithms detailed in Section 4.2.

The subsequent path following ensures precise navigation along the planned collision-free path, effectively avoiding obstacles for safe operation. The core idea, illustrated in Figure 19a, is to track a virtual reference vehicle moving along the planned path with coordinates  $\mathbf{q}^d = [x^d, y^d, \theta^d]^T$ , which corresponds to the input of the vehicle base control structure described in (4)-(6). The position of the virtual reference vehicle is calculated by identifying the closest pose on the path to the actual vehicle pose  $\mathbf{q}_{F/R} = [x_{F/R}, y_{F/R}, \theta_{F/R}]^T$ , depending on forward (F) or reverse (R) driving and, from this pose on, simulating a movement along the path for a specified look-ahead distance. This distance determines how far ahead the vehicle anticipates along the path, balancing responsiveness and stability for smooth and accurate path following. The pose resulting in the path after this simulated movement serves as the reference pose  $\mathbf{q}^d$  for tracking the path.

Since the forklift is designed to operate in both forward and reverse driving directions and the implemented path tracking control law is designed for uni-directional movement, the bi-directional path following approach employs a multi-stage approach. The bi-directional path consists of segments, separated by turning poses, with alternating movement direction. Therefore, the respective vehicle pose also alternates between the front  $\mathbf{q}_F$  and the rear axle  $\mathbf{q}_R$ . This approach is facilitated by the forklift's symmetric geometry and smooth transitions between the segments are handled by the behavior tree. An example of bi-directional path following, including a turning pose, is shown in Figure 18.

In addition to controlling the vehicle base, the path-following module utilizes the simplified fork control loop, see Figure 16b, without FTT) to ensure that the forks maintain a safe height and angle, particularly when trans-



(a) Concept for path following, showing the virtual vehicle  $\mathbf{q}^d = [x^d, y^d, \theta^d]^T$  as the reference pose.

(b) Pallet manipulation scenario, showing the rear of the vehicle  $\mathbf{q}_R = [x_R, y_R, \theta_R]^T$ , the pallet pose  $\mathbf{q}_P = [x_P, y_P, \theta_P, z_P]^T$  and the tip of the forks  $\mathbf{q}_T = [x_T, y_T, \theta_T, z_T]^T$ .

Figure 19: Concepts for path following and pallet manipulation.

porting a load. This is achieved by directly applying the predefined setpoint values  $l^d$ ,  $s^d$  and  $\beta^d$  for the respective joints.

### 5.3.3. Manipulation

The *Manipulation* action involves the correct pick-up and drop-off of the pallets. The high-level task planning framework controls this action by selecting a suitable target pallet based on spatial proximity and accessibility and then executing a controlled approach. To ensure correct pallet pickup, both the vehicle base and fork cascaded control loops from Section 5.3.1 are necessary. The aim is to minimize the error between the pallet pose and the vehicle's rear axle. The target pose for the vehicle base control is now the center of the front face of the pallet ( $\mathbf{q}^d = \mathbf{q}_P$ ) and the vehicle origin is the center of the rear axle  $\mathbf{q}_R^3$ , as illustrated in Figure 19b.

During the pallet approach phase, the FTT component from Figure 16b is crucial to align the fork tips with the pallet openings, before and while the vehicle is moving onto the pallet. The reverse action of placing the pallet follows a process similar to pickup. Here, a virtual pallet called *slot* defines the target location, guiding the system to the desired position. Figure 20 illustrates data from a successful pallet manipulation maneuver, showing the process of placing a pallet into a slot on the truck. The critical moment for loading the pallet, highlighted by a dashed gray line, occurs when the fork tips reach the front of the (virtual) pallet, and the forks must properly engage with the pallet pockets. The vehicle stops moving ( $v^d = 0$ ) at  $x'_P = -d_F$ , where  $d_F$  corresponds to the length of the

forks or if the fork-mounted laser sensor indicates successful pallet insertion.

Initial iterations of ADAPT have shown that placing the pallet on its designated slot purely by estimating its z-position based on the ground plane or a truck loading edge is not sufficiently robust. Thus, we introduce a simple improvement procedure based on measuring the hydraulic pressure in the fork lifting cylinder, as follows:

1. The forklift enters the selected slot at a safe height above the estimated pose.
2. After reaching the desired pose in x and y, the vehicle stops.
3. The forks are slowly lowered until the hydraulic pressure of the lifting cylinder drops, indicating that the fork is in contact with the underlying ground.
4. Finally, the fork is lifted again by half the height of the pallet to safely retract from the pallet.

The method for estimating the fork contact  $f_c$  is explained in Algorithm 1. A graphical description based on exem-

---

#### Algorithm 1 Fork contact detection.

---

**Input:** Lifting pressure  $p_l$ .

**Output:**  $f_c$ : *true* if fork in contact, *false* otherwise.

---

- 1: **if**  $p \leq p_{pc}$  **then**
  - 2:      $crit\_cnt \leftarrow crit\_cnt + 1$ ,  $f_{pc} \leftarrow true$
  - 3: **else**
  - 4:      $crit\_cnt \leftarrow 0$ ,  $f_{pc} \leftarrow false$
  - 5: **end if**
  - 6: **if**  $crit\_cnt > crit\_tout$  **or**  $p_l < p_c$  **then**
  - 7:      $f_c \leftarrow true$ ,  $f_{pc} \leftarrow true$
  - 8: **else**
  - 9:      $f_c \leftarrow false$
  - 10: **end if**
- 

<sup>3</sup>Remember that the forks are mounted at the rear of the vehicle.

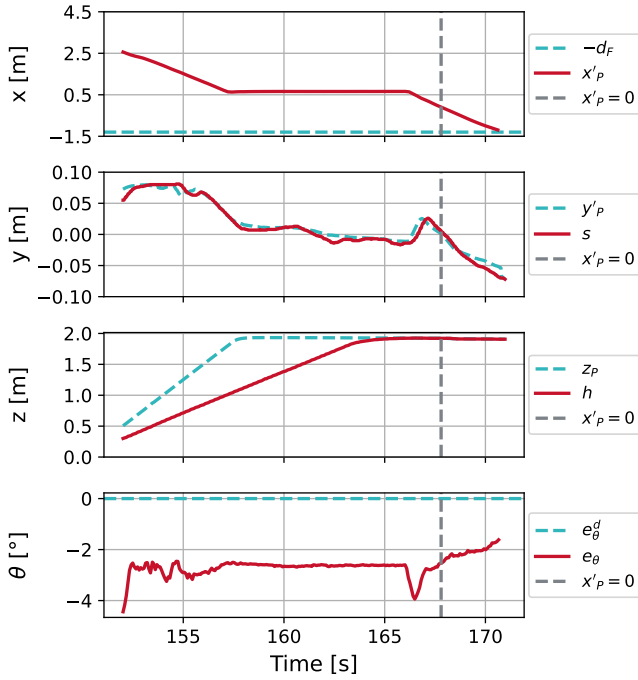


Figure 20: Exemplary data for placing a pallet in a slot on the truck. Cyan lines indicate setpoint signals, red lines measurements, and the gray dashed line marks the time when the fork tip reaches the front of the slot. The standstill time ( $\dot{x}_p = 0$ ) of  $\approx 10$  seconds results from the waiting time required for the forks to reach the desired height.

playa pallet unloading measurements is shown in Figure 21. In addition to ensuring that a pallet is placed at the correct height, this method also serves as a safety feature to prevent dangerous downward fork movement in case the forks come into contact with the environment. The threshold levels indicating possible ( $p_{pc}$ ) and definite fork contact ( $p_c$ ) are empirically selected as a trade-off between operational robustness and safety.

## 6. Validation and Evaluation

This section describes the experimental setup in our outdoor large-scale robotics lab followed by a detailed analysis of the robust long-term operation together with a direct comparison with an experienced human operator. At the end, lessons learnt of the development and testing process are presented to improve development for future work.

### 6.1. Experimental Setup

The experiment is designed to evaluate the long-term operational robustness and performance of ADAPT across close-to-real loading scenarios. Three distinct operational modes were tested: ground-to-ground (G to G) pallet loading, ground-to-truck (G to T) pallet loading, and truck-to-ground (T to G) pallet unloading. In this context, the experimental setup involved a truck loaded with four Euro-pallets, each carrying varying types of loads to simulate real-world handling conditions. The initial location for the

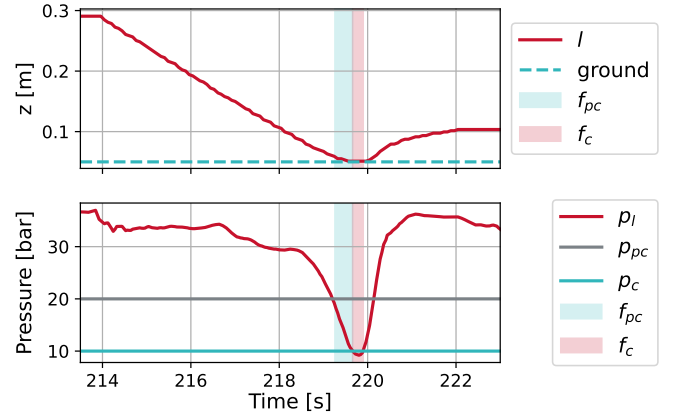


Figure 21: Fork contact detection. Hydraulic pressure in the lifting cylinder  $p_l$  below a certain level indicates fork contact with environment ( $f_c = true$ ). The threshold levels indicate possible fork contact ( $p_{pc}$ ) and definite fork contact ( $p_c$ ).

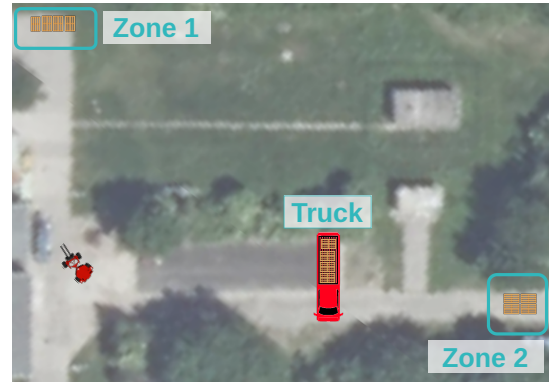


Figure 22: Satellite image showing the test site with an overlay for the configuration of the loading zones (Zone 1 & Zone 2) as well as the truck location used for the experiments.

forklift and the truck parking location are unchanged in all experiments, to allow for a fair comparison between baseline data collected from an expert operator and data collected from autonomous operation. Figure 22 shows the test site with an overlay of the configuration of the ground loading zones (Zone 1 & Zone 2) as well as the truck location.

Note that neither the ground loading zones nor the truck have predefined pallet positions. Pallets can be placed anywhere within these areas, with the restriction that they must be accessible by the forklift. Example situations for ground loading zones are shown in Figure 23 from the view of the pallet detector camera on top of the lift mast. For unloading in Zone 1, all four pallets were arranged in a single row, whereas in Zone 2 they were arranged in two rows with two pallets in each row.

As noted above, one of the purposes of this work is to evaluate the automated system under varying weather conditions. Therefore, the baseline data, as well as the data from autonomous operation, are collected under different weather conditions including sunny, cloudy, and rainy





Figure 23: Pallets from the camera on top of the lift mast for Zone 1 (left) and 2 (right).



Figure 24: Rainy environment conditions for the ground to ground scenario with reflective puddles.

weather. All ground-to-ground loading scenarios were carried out in rainy conditions as illustrated in Fig. 24.

### 6.2. Baseline data collection

To be able to assess the efficiency, accuracy and general performance of the autonomous forklift during typical loading scenarios, data from manual operation were collected. The baseline data was collected through an experienced and external forklift operator with more than 20 years of experience in handling this type of forklift. The data collection process was supervised by an engineering team over a three-day period, encompassing a variety of weather conditions. The study included multiple test scenarios, covering both loading and unloading from a truck as well as ground-level pallet handling. Each scenario was repeated across several cycles to generate statistically significant results. Overall, 280 minutes of consecutive driving were collected.

### 6.3. Performance Criteria

To compare the performance of ADAPT with an experienced operator, manual operation was recorded with the same forklift. The maximum velocity in autonomous operation was limited to the legally maximum allowed velocity of  $v_{max} = 6\text{km/h}$ . The following performance criteria are selected for evaluation:

**Time Taken for Full Loading Cycle:** Total time taken to complete the entire pallet loading and unloading process, from the first pallet pick-up to the last pallet placement. This provides a direct measure of throughput,

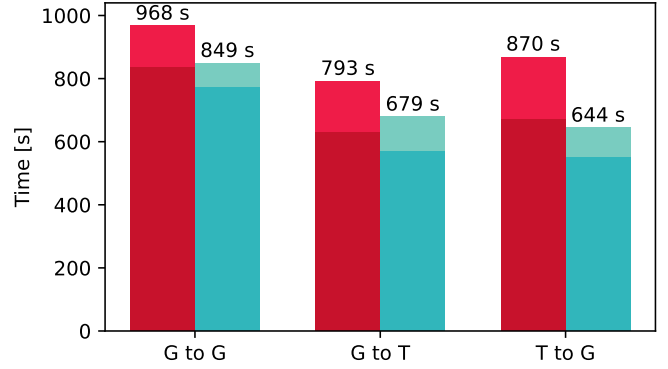


Figure 25: Overall mean time for the three scenarios ground-to-ground (G to G), ground-to-truck (G to T) and truck-to-ground (T to G) for autonomous operation (red) and the expert operator (turquoise). Time spent driving in darker, standstill in lighter color.

allowing a clear comparison of speed and productivity between the automated system and the human operator.

**Distance Driven:** Total distance traveled for the full load task. This enables a comparison between the route efficiency of the automated system's algorithms and the decision-making of an expert operator. Lower travel distances also equal less energy consumption.

**Manual Interventions:** Quantity and severity of manual interventions required during autonomous operation. The goal is to analyze the autonomy of the system and its need of human involvement to correct errors, manage obstacles, or ensure safety.

Using these criteria, it is possible to conduct a comprehensive, quantitative and qualitative comparison of ADAPT and an expert operator, with an emphasis on efficiency and operational performance.

### 6.4. Performance Analysis

**Time Taken for Full Loading Cycle:** Figure 25 compares the overall task completion times for autonomous and manual operations across three scenarios: ground-to-ground (G to G), ground-to-truck (G to T), and truck-to-ground (T to G). The figure further distinguishes between time spent driving (shown in a darker shade) and non-driving task execution (shown in a lighter shade). Overall, the experienced operator completed the loading tasks in 82.5% of the time required by ADAPT.

In the simpler G to G scenario, the autonomous system achieves approximately 88% of expert-level performance, demonstrating its strong potential for timely deployment in commercial operations. In the more complex task of loading onto the truck, the autonomous system remains competitive, showing a time difference of 14% compared to the performance of experts. The largest discrepancy, 26%, is observed in the loading-from-truck scenario. The extended standstill times observed in ADAPT primarily result from computational and detection delays, as well as inefficiencies associated with the sequential execution of tasks, as discussed in detail later.



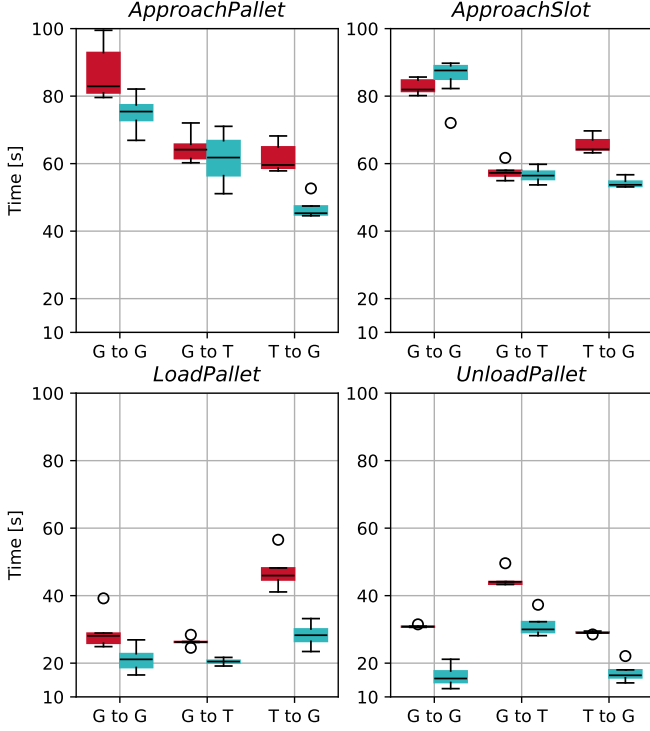


Figure 26: Time evaluation of the sub-missions for ground-to-ground (G to G), ground-to-truck (G to T) and truck-to-ground (T to G) loading for autonomous operation (red) and the forklift operator (cyan).

To evaluate the potential for performance and improvement in more detail, Figure 26 provides a statistical time analysis based on the subtasks of autonomous operation. The missions are defined as discussed in Section 5 as *ApproachPallet*, *LoadPallet*, *ApproachSlot* and *UnloadPallet*. The two submissions *FindPallets* and *SelectPallets* are included in *ApproachPallet* to increase readability. The two *Approach* missions consist mostly of typical navigation movement, whereas the load and unload missions deal mostly with manipulation.

For the *ApproachPallet*, a longer time and a higher variance for ADAPT can be observed. This arises mostly from two properties of the pallet detection: Firstly, when no pallets are known to the system, ADAPT stops for several seconds in front of the loading zone to obtain a stable object list. Secondly, as the position and orientation of the pallets are not known in advance, a new approach of pallets is sometimes mandatory for correct loading which takes up to 30 seconds. Especially for the G to G scenario, this occurred multiple times resulting in the larger variance for the approach. In the G to T case, the performance of ADAPT and the expert is very similar because the expert operator chooses a suboptimal path as detailed in the latter. For the *ApproachSlot* mission, ADAPT achieves a very similar performance, even though more changes in driving direction were made.

For the manipulation subtasks, ADAPT performs very consistently for all scenarios. For loading, the performance

of G to G and G to T is very similar to that of the human operator. The loading of the truck takes longer for ADAPT. This mostly arises from the time needed to raise the forks to the height of the loading platform and the additional pallet detection check when the pallet is located in a plane different from the movement plane. The unloading of the pallets is close to a standardized task and thus can be done with accurate timing with hardly any variance by the autonomous system. The key difference from manual operation is that the autonomous system raises the forks while stationary, as shown in Figure 20, while a human operator simultaneously manipulates the forks and drives to maximize efficiency. This illustrates a case where ADAPT is not yet optimized for timing performance.

**Distance Driven:** Figure 27 illustrates an overlay of the manual and autonomous paths for a representative loading cycle in each scenario. In general, it can be observed that the expert operator shows a superior utilization of the free space available for turning compared to the autonomous planning system. This results in fewer changes in driving direction during manual operation. In contrast, the autonomous vehicle tends to navigate closer to obstacles, such as bushes, allowing it to effectively cut corners. These opposing behaviors nearly compensate for each other, resulting in comparable path lengths, as summarized in Figure 28. Contrary to our intuition, the expert operator performs impressively consistent with a very low variance of the path length. For ADAPT, the variance in path length is greater as a result of the heuristic nature of the hybrid A\* path planner. This can also be seen in the plotted paths in Figure 27, where the paths of the human operator are impressively equal within one scenario.

Across different scenarios, a notable change in human operator behavior was observed, see Figure 27. After the first recorded scenario, ground-to-truck loading, the expert operator adapted his turning strategy. Instead of turning immediately after loading, the operator used the corner as a natural pivot point to change the driving direction. This adjustment was shown to be significantly faster, as evidenced by the reduced driving time in the *ApproachPallet* phase compared to the truck-to-ground scenario. These observations highlight the dependency of performance on the skill level of the forklift operator. Less skilled operators not only take longer to load and unload pallets but also tend to select suboptimal driving paths, further impacting overall efficiency.

**Manual Interventions:** During the recorded operation period of more than 3 hours of autonomous functionality, during which 60 pallets were loaded, a total of 17 manual interventions were required. These manual interventions were classified into three categories: Collision Detection, Manipulation and Navigation. The distribution of types of manual intervention is illustrated on the left-hand side of Figure 29.

Notably, nearly 60% of these interventions were attributed to the collision avoidance module, which requires human clearance for any detected potential collision. Many

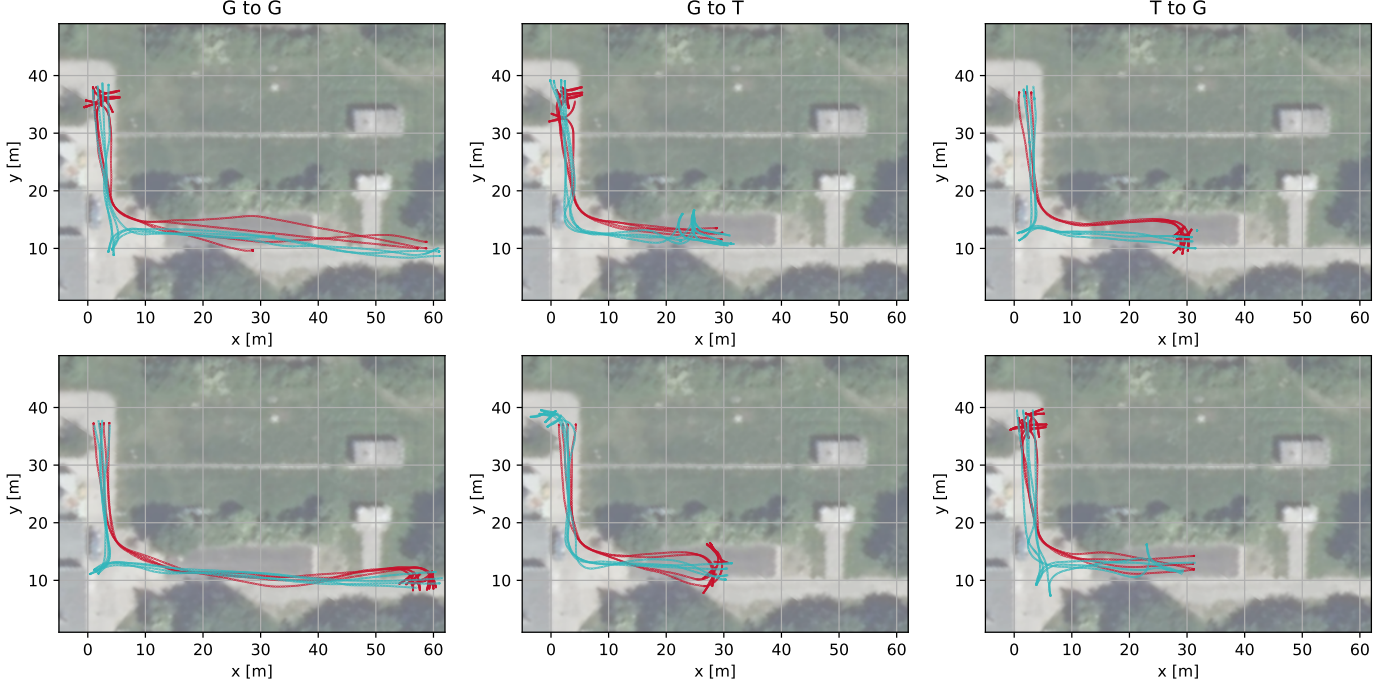


Figure 27: Paths for autonomous (red) and manual (cyan) operation for all 3 scenarios for *ApproachPallet* (top) and *ApproachSlot* (bottom).

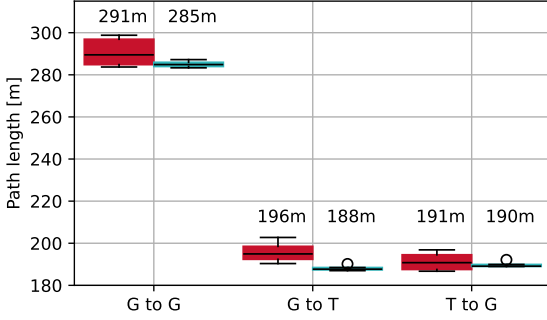


Figure 28: Path length evaluation for autonomous (red) and manual (turquoise) operation. Text denotes the absolute path length.

of these collision warnings occurred near the boundary of the map, where the distance from the collision is shorter if approaching an obstacle or boundary of the map. This issue, resulting from stringent safety constraints in the laboratory environment, could potentially be alleviated by implementing obstacle-classification-based warning distances, assigning larger safety margins for humans and moving obstacles, and smaller margins for static obstacles. Additionally, collision warnings were correctly triggered when humans, including the safety operator, were detected in the vehicle's path, although such incidents were rare. The second category involves inaccuracies in the detection and manipulation modules, which result in failed pallet load and unload attempts. Implementing recovery routines could reduce the number of necessary manual interventions, albeit at the cost of longer execution times. Lastly, navigation and localization interventions occur when no path to a desired position could be planned or when the localization

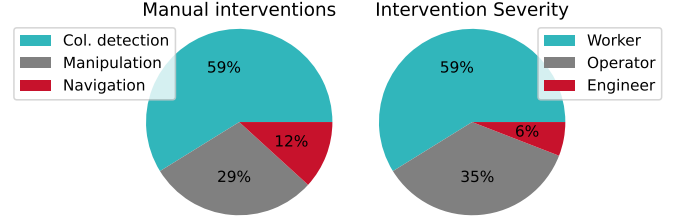


Figure 29: Overall manual interventions for the autonomous loading operation categorized for their type and their intervention severity.

module fails. On the right-hand side of Figure 29, the severity of manual interventions is classified. To this end, three categories of expertise are introduced: 1) *Worker* for a typical worker on site with little knowledge of the machine, 2) *Operator* which denotes an educated forklift operator capable of driving the machine manually and 3) *Engineer* as a robotic engineer with in-depth knowledge of the autonomy framework. Most interventions can be handled by a regular worker by simply ensuring that the corridor in front of the autonomous vehicle is free of obstacles. For ADAPT this is verified by pressing a conformation button once. Approximately one third of interventions require an operator for forklift operations to assist in navigation or manipulation. In our tests, there was one instance where an engineer with knowledge of the autonomous functions was needed, due to a failure in the GNSS localization system. Fig. 30 presents the time analysis of manual interventions during autonomous operation. During a total of 233 minutes of autonomous operation, only 12 minutes were spent in manual control, accounting for less than 5% of the total

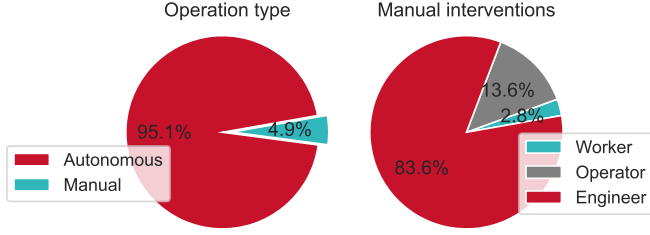


Figure 30: Left: Time spent on autonomous operation (red) compared to manual interventions (cyan). Right: Time spent for the manual interventions categories in severity.

operation time. Most of this manual intervention, 10 minutes, was dedicated to resolving a GNSS localization issue, which is primarily a prototype-related challenge. All other combined manual interventions accounted for just 2 minutes, representing less than 1% of the total operation time. These results highlight the substantial reduction in manual labor required for material transport, demonstrating the efficiency of ADAPT.

### 6.5. Lessons Learned

This section outlines key lessons learned from the development and testing of ADAPT, providing insights that we hope will assist fellow researchers in the advancement of autonomous machine technology and the enhancement of the reliability of the system.

**All-weather Operation:** The initial iteration of our collision avoidance system was based on a wide-angle stereo camera and was tested in an artificial outdoor rain facility designed for autonomous vehicle evaluation. The tests showed that our system performed better in rainy conditions than comparable LiDAR-based solutions, probably due to algorithmic advantages (*i.e.*, a stereo-based rain filter) and mechanical rain protection. For the current iteration, we integrated a LiDAR system with overhead rain protection. Its wider field of view enhances obstacle detection and enables mapping, which stereo cameras alone cannot provide. Additionally, the stereo camera system faced reliability issues in sub-zero temperatures due to USB controller failures, which were mitigated by switching to LiDAR.

In contrast, at high temperatures (above 30°C), we encountered overheating problems with an earlier iteration of the switch cabinet, as its unavoidable placement near the exhaust of the diesel engine exposed it to excessive heat. The current design addresses this problem with an improved inlet for air flow required by the active air-cooling system.

**RTK Evaluation:** During an earlier system iteration, inconsistent RTK positioning was observed. Extensive investigation revealed that the vehicle’s internal environment contributed significantly to signal interference. Notably, reducing the number of active electronic devices — particularly a USB 3.0 stereo camera connected via a 5-meter cable — mitigated interference. Further research showed

that USB 3.0 devices can disrupt GNSS signals, see, *e.g.*, [80]. The replacement of the USB 3.0 cable with a fiber optic cable for data transmission while maintaining a metallic power supply effectively eliminated interference, leading to a significant improvement in the reliability of the RTK positioning.

**Multi-sensor Calibration:** The factory ZED2i calibration did not meet our needs in terms of accuracy, hence intrinsic camera and stereo calibration have been performed with our proprietary calibration pipeline. In addition, semi-automatic sensor-to-sensor calibrations save time during hardware iterations and can be used to correct aging drift.

**Positioning Accuracy:** A measurement campaign revealed that in 80% of unloading cases, the global positioning accuracy of ADAPT was sufficient to unload pallets within a 5 cm tolerance without requiring additional local measurements. However, the remaining 20% cases require the continued use of additional local correction mechanisms, such as repeated loading edge detection or local control mechanisms that rely on the LiDAR sensor mounted on a fork.

**Simulative Verification and Testing:** A significant part of the development and testing of autonomous functionality for ADAPT was carried out in simulation environments. The initial approach aimed for a holistic simulation to test all functionalities in one environment. However, this proved counterproductive, as different tasks have distinct requirements (*e.g.*, photorealism for perception versus real physics for motion control). To address this, specialized simulation tools were used: Gazebo<sup>4</sup> for task and motion planning and control algorithms, and Blender<sup>5</sup> for object detection evaluation. This approach offered a cost-effective and safe way to validate autonomous functionalities before real-world deployment, especially considering the extensive setup time for prototype tests. Another advantage of simulation was the isolated testing of individual functions, which improved the identification of error sources and was often challenging on the real prototype.

## 7. Conclusion and Outlook

This article presented the autonomous outdoor forklift ADAPT, a system capable of operating in the complex and unstructured environments of construction sites, even in challenging conditions, including low to medium rain. By integrating a forklift-specific sensor suite with a tailored software stack, the system achieves fully autonomous pallet loading and transportation. Extensive real-world testing demonstrated that the autonomous forklift operates at near-human efficiency, achieving more than 80% of expert level performance in the demonstrated scenarios, while requiring minimal operator intervention.

A key contribution of this work is the novel factor-graph-based joint optimization approach for vehicle localization

<sup>4</sup><https://classic.gazebosim.org> (accessed 2025-02-28)

<sup>5</sup><https://www.blender.org> (accessed 2025-02-28)

and pallet mapping, specifically tailored for object manipulation tasks such as pallet loading. This method enhances the system's adaptability and accuracy in dynamic construction site environments. Additionally, the integration of a novel fork contact measurement based on pressure feedback significantly improves robustness and safety during object manipulation while remaining cost-effective and simple to implement.

A detailed long-term evaluation compared the autonomous forklift's performance to that of an expert human operator with over 20 years of experience. The analysis provided insights into performance, robustness, and the nature and frequency of required human interventions. These findings highlight the system's potential to improve efficiency and safety in material handling for construction sites, addressing labor shortages and reducing operational risks.

Future improvements will focus on motion planning in dynamic environments to enhance safety while maintaining operational efficiency. Additionally, the incorporation of semantic information into the environment mapping approach will complement the existing geometric model, allowing the forklift to prioritize stable surfaces such as concrete roads over more challenging terrains like gravel or soil. Further efforts will be directed toward increasing robustness when navigating through challenging terrain and extreme weather conditions. Recurring hardware updates, particularly those involving processing components, will allow for either replacing existing hardware with more compact, resource-efficient alternatives or utilizing higher-performance components to improve overall timing-related performance. By addressing these aspects, the system can continue to evolve toward a fully integrated, intelligent solution for autonomous material handling in demanding construction environments.

## CRedit authorship contribution statement

**Johannes Huemer:** Writing – Original Draft, Methodology, Conceptualization, Software, Hardware. **Markus Murschitz:** Conceptualization, Supervision, Writing – Original Draft, Methodology, Software. **Benedikt Widy:** Methodology, Hardware. **Matthias Schörghuber:** Writing – Original Draft, Methodology, Software. **Marcel Zeilinger:** Methodology, Software. **Thomas Kadiofsky:** Writing – Original Draft, Methodology, Software. **Christoph Weidinger:** Methodology, Software. **Lukas Reisinger:** Methodology, Software, Data curation. **Csaba Beleznai:** Writing – Original Draft, Methodology, Data curation. **Mario Niedermeyer:** Software, Hardware, Validation. **Tobias Glück:** Writing - Review & Editing, Funding acquisition. **Andreas Kugi:** Writing - Review & Editing, Funding acquisition. **Patrik Zips:** Writing – Original Draft, Methodology, Formal analysis, Investigation, Project administration.

## Declaration of competing interest

The authors declare that they have no known competing financial interests or personal relationships that could have appeared to influence the work reported in this paper.

## Declaration of generative AI and AI-assisted technologies in the writing process

During the preparation of this work the authors used ChatGPT and DeepL to improve the readability and reduce spelling errors. After using this tool, the authors reviewed and edited the content as needed and take full responsibility for the content of the published article.

## Acknowledgments

This work was funded by the European Union's Horizon 2020 research and innovation program under Grant Agreement No. 101006817. Additionally, it received support from the Austrian Research Promotion Agency (FFG) through the ICT of the Future program under Project No. 873987. We would also like to express our gratitude to our collaboration partners FH OÖ, Wolfgang Pointner, and Palfinger as well as Florian Wimmer for the initial version of the loading platform detection.

## References

- [1] C. H. Caldas, C. L. Menches, P. M. Reyes, L. Navarro, and D. M. Vargas, "Materials Management Practices in the Construction Industry," *Practice Periodical on Structural Design and Construction*, vol. 20, no. 3, p. 04014039, 2015.
- [2] H. R. Thomas, D. R. Riley, and J. I. Messner, "Fundamental Principles of Site Material Management," *Journal of Construction Engineering and Management*, vol. 131, no. 7, pp. 808–815, 2005.
- [3] S. Donyavi and R. Flanagan, "The impact of effective material management on construction site performance for small and medium sized construction enterprises," in *Proceedings of the 25th Annual ARCOM Conference, Nottingham, UK, 2009*, pp. 11–20.
- [4] Khursheed, Salman, Sharma, Sumit, Paul, Virendra Kumar, Alzubaidi, Laith H, and Israilova, Dildora, "Review of the Factors Inducing Delay in Construction Project Material Management," *E3S Web Conf.*, vol. 563, p. 02044, 2024.
- [5] G. Barbosa, F. Andrade, C. Biotto, and B. Mota, "Heijunka system to level telescopic forklift activities using tablets in construction site," in *Proc. of XXI IGLC Ann. Conf.*, 2013, pp. 821–830.
- [6] R. L. Neitzel, N. S. Seixas, and K. K. Ren, "A Review of Crane Safety in the Construction Industry," *Applied Occupational and Environmental Hygiene*, vol. 16, no. 12, pp. 1106–1117, 2001.
- [7] D. Jud, S. Kerscher, M. Wermelinger, E. Jelavic, P. Egli, P. Leemann, G. Hottiger, and M. Hutter, "HEAP - The autonomous walking excavator," *Automation in Construction*, vol. 129, p. 103783, 2021.
- [8] E. Jelavic, T. Kapgen, S. Kerscher, D. Jud, and M. Hutter, "Harveri: A Small (Semi-)Autonomous Precision Tree Harvester," ETH Zurich, 2022.
- [9] R. Meyer, "The Journey to Regular Operation of a Fully Automatic Terminal Tractor at a Depot in Mixed Operation," in *Automatisiertes Fahren 2024*, A. Heintzel, Ed. Wiesbaden: Springer Fachmedien Wiesbaden, 2024, pp. 63–76.

- [10] A. Tews, C. Pradalier, and J. Roberts, "Autonomous Hot Metal Carrier," in *Proceedings 2007 IEEE International Conference on Robotics and Automation*, 2007, pp. 1176–1182.
- [11] T. A. Tamba, B. Hong, and K.-S. Hong, "A path following control of an unmanned autonomous forklift," *International Journal of Control, Automation and Systems*, vol. 7, no. 1, pp. 113–122, 2009.
- [12] M. R. Walter, M. Antone, E. Chuangsuwanich, A. Correa, R. Davis, L. Fletcher, E. Frazzoli, Y. Friedman, J. Glass, J. P. How *et al.*, "A Situationally Aware Voice-commandable Robotic Forklift Working Alongside People in Unstructured Outdoor Environments," *Journal of Field Robotics*, vol. 32, no. 4, pp. 590–628, 2015.
- [13] R. Iinuma, Y. Kojima, H. Onoyama, T. Fukao, S. Hattori, and Y. Nonogaki, "Pallet Handling System with an Autonomous Forklift for Outdoor Fields," *Journal of Robotics and Mechatronics*, vol. 32, no. 5, pp. 1071–1079, 2020.
- [14] "On the path to autonomous outdoor operation of forklift trucks," <https://www.kiongroup.com/en/News-Stories/Stories/Automation/On-the-path-to-autonomous-outdoor-operation-of-forklift-trucks.html>, [Accessed February 25, 2025].
- [15] M. G. Dissanayake, P. Newman, S. Clark, H. F. Durrant-Whyte, and M. Csorba, "A solution to the simultaneous localization and map building (SLAM) problem," *IEEE Transactions on robotics and automation*, vol. 17, no. 3, pp. 229–241, 2001.
- [16] C. Cadena, L. Carlone, H. Carrillo, Y. Latif, D. Scaramuzza, J. Neira, I. Reid, and J. J. Leonard, "Past, present, and future of simultaneous localization and mapping: Toward the robust-perception age," *IEEE Transactions on robotics*, vol. 32, no. 6, pp. 1309–1332, 2016.
- [17] K. Ebadi, L. Bernreiter, H. Biggie, G. Catt, Y. Chang, A. Chatterjee, C. E. Denniston, S.-P. Deschênes, K. Harlow, S. Khattak, L. Nogueira, M. Palieri, P. Petráček, M. Petrlik, A. Reinke, V. Krátký, S. Zhao, A.-a. Agha-mohammadi, K. Alexis, C. Heckman, K. Khosoussi, N. Kottege, B. Morrell, M. Hutter, F. Pauling, F. Pomerleau, M. Saska, S. Scherer, R. Siegwart, J. L. Williams, and L. Carlone, "Present and future of slam in extreme environments: The darpa sub challenge," *IEEE Transactions on Robotics*, vol. 40, pp. 936–959, 2024.
- [18] F. Wang, E. Lü, Y. Wang, G. Qiu, and H. Lu, "Efficient Stereo Visual Simultaneous Localization and Mapping for an Autonomous Unmanned Forklift in an Unstructured Warehouse," *Applied Sciences*, vol. 10, no. 2, 2020.
- [19] A. Hornung, K. M. Wurm, M. Bennewitz, C. Stachniss, and W. Burgard, "OctoMap: an efficient probabilistic 3D mapping framework based on octrees," *Autonomous Robots*, vol. 34, no. 3, pp. 189–206, 2013.
- [20] S. Macenski, D. Tsai, and M. Feinberg, "Spatio-temporal voxel layer: A view on robot perception for the dynamic world," *International Journal of Advanced Robotic Systems*, vol. 17, no. 2, 2020.
- [21] M. G. Besselmann, L. Puck, L. Steffen, A. Roennau, and R. Dillmann, "VDB-Mapping: A High Resolution and Real-Time Capable 3D Mapping Framework for Versatile Mobile Robots," in *2021 IEEE 17th International Conference on Automation Science and Engineering (CASE)*, 2021, pp. 448–454.
- [22] P. Krüsi, P. Furgale, M. Bosse, and R. Siegwart, "Driving on Point Clouds: Motion Planning, Trajectory Optimization, and Terrain Assessment in Generic Nonplanar Environments," *Journal of Field Robotics*, vol. 34, no. 5, pp. 940–984, 2017.
- [23] T. Whelan, M. Kaess, H. Johannsson, M. Fallon, J. J. Leonard, and J. McDonald, "Real-time large-scale dense RGB-D SLAM with volumetric fusion," *The International Journal of Robotics Research*, vol. 34, no. 4-5, pp. 598–626, 2015.
- [24] H. Oleynikova, Z. Taylor, M. Fehr, J. Nieto, and R. Siegwart, "Voxblox: Incremental 3D Euclidean Signed Distance Fields for On-Board MAV Planning," in *2017 IEEE/RSJ International Conference on Intelligent Robots and Systems (IROS)*, 2017, pp. 1366–1373.
- [25] I. Vizzo, T. Guadagnino, J. Behley, and C. Stachniss, "VDBFu- sion: Flexible and Efficient TSDF Integration of Range Sensor Data," *Sensors*, vol. 22, no. 3, p. 1296, 2022.
- [26] P. Borges, T. Peynot, S. Liang, B. Arain, M. Wildie, M. Minareci, S. Lichman, G. Samvedi, I. Sa, N. Hudson, M. Milford, P. Moghadam, and P. Corke, "A Survey on Terrain Traversability Analysis for Autonomous Ground Vehicles: Methods, Sensors, and Challenges," *Field Robotics*, vol. 2, no. 1, pp. 1567–1627, 2022.
- [27] D. J. Yeong, G. Velasco-Hernandez, J. Barry, and J. Walsh, "Sensor and sensor fusion technology in autonomous vehicles: A review," *Sensors*, vol. 21, no. 6, p. 2140, 2021.
- [28] M. N. Ahangar, Q. Z. Ahmed, F. A. Khan, and M. Hafeez, "A survey of autonomous vehicles: Enabling communication technologies and challenges," *Sensors*, vol. 21, no. 3, p. 706, 2021.
- [29] F. Dellaert, M. Kaess *et al.*, "Factor graphs for robot perception," *Foundations and Trends® in Robotics*, vol. 6, no. 1-2, pp. 1–139, 2017.
- [30] R. Jung and S. Weiss, "Modular multi-sensor fusion: A collaborative state estimation perspective," *IEEE Robotics and Automation Letters*, vol. 6, no. 4, pp. 6891–6898, 2021.
- [31] W. Talbot, J. Nubert, T. Tuna, C. Cadena, F. Dümbsen, J. Tordesillas, T. D. Barfoot, and M. Hutter, "Continuous-time state estimation methods in robotics: A survey," 2024.
- [32] J. Nubert, S. Khattak, and M. Hutter, "Graph-based multi-sensor fusion for consistent localization of autonomous construction robots," in *IEEE International Conference on Robotics and Automation (ICRA)*, 2022, pp. 10 048–10 054.
- [33] M. Kaess, H. Johannsson, R. Roberts, V. Ila, J. J. Leonard, and F. Dellaert, "iSAM2: Incremental smoothing and mapping using the Bayes tree," *The International Journal of Robotics Research*, vol. 31, no. 2, pp. 216–235, 2012.
- [34] J. Xiao, H. Lu, L. Zhang, and J. Zhang, "Pallet recognition and localization using an RGB-D camera," *International Journal of Advanced Robotic Systems*, vol. 14, 2017.
- [35] Y. Shao, Z. Fan, B. Zhu, J. Lu, and Y. Lang, "A Point Cloud Data-Driven Pallet Pose Estimation Method Using an Active Binocular Vision Sensor," *Sensors*, vol. 23, no. 3, 2023.
- [36] M. Sundermeyer, T. Hodaň, Y. Labbé, G. Wang, E. Brachmann, B. Drost, C. Rother, and J. Matas, "BOP Challenge 2022 on Detection, Segmentation and Pose Estimation of Specific Rigid Objects," in *IEEE Computer Society Conference on Computer Vision and Pattern Recognition Workshops*, 2023, pp. 2785–2794.
- [37] V.-D. Vu, D.-D. Hoang, P. Tan, V.-T. Nguyen, T.-U. Nguyen, N.-A. Hoang, K.-T. Phan, D.-T. Tran, D.-Q. Vu, P.-Q. Ngo, Q.-T. Duong, N. Nhat, and D.-C. Hoang, "Occlusion-Robust Pallet Pose Estimation for Warehouse Automation," *IEEE Access*, vol. 12, pp. 1927–1942, 2024.
- [38] NVIDIA-AI-IOT, "SDG Pallet Model," [https://github.com/NVIDIA-AI-IOT/sdg\\_pallet\\_model/](https://github.com/NVIDIA-AI-IOT/sdg_pallet_model/), 2023, [Accessed January 16, 2025].
- [39] N. Kai, H. Yoshida, and T. Shibata, "Pallet Pose Estimation Based on Front Face Shot," *IEEE Access*, 2025.
- [40] C. Beleznaï, L. Reisinger, W. Pointner, and M. Murschitz, "Pallet detection and 3D pose estimation via geometric cues learned from synthetic data," in *Proceedings of the 4th International Conference on Pattern Recognition and Artificial Intelligence, ICPRAI 2024*. Springer Singapore, Dec. 2024, pp. 281–295.
- [41] R. Ghzouli, T. Berger, E. B. Johnsen, A. Wasowski, and S. Dragule, "Behavior Trees and State Machines in Robotics Applications," *IEEE Transactions on Software Engineering*, vol. 49, no. 9, pp. 4243–4267, 2023.
- [42] C. R. Garrett, R. Chitnis, R. Holladay, B. Kim, T. Silver, L. P. Kaelbling, and T. Lozano-Pérez, "Integrated Task and Motion Planning," *Annual Review of Control, Robotics, and Autonomous Systems*, vol. 4, no. 1, pp. 265–293, 2021.
- [43] V. N. Hartmann, O. S. Oguz, D. Driess, M. Toussaint, and A. Menges, "Robust Task and Motion Planning for Long-Horizon Architectural Construction Planning," in *2020 IEEE/RSJ International Conference on Intelligent Robots and Systems (IROS)*, 2020, pp. 6886–6893.



- [44] S. Li, D. Park, Y. Sung, J. A. Shah, and N. Roy, "Reactive Task and Motion Planning under Temporal Logic Specifications," in *2021 IEEE International Conference on Robotics and Automation (ICRA)*. IEEE Press, 2021, pp. 12 618–12 624.
- [45] J. Huang, A. Tao, R. Marco, M. Bogdanovic, J. Kelly, and F. Shkurti, "Automated Planning Domain Inference for Task and Motion Planning," *arXiv preprint arXiv:2410.16445*, 2024.
- [46] T. Birr, C. Pohl, A. Younes, and T. Asfour, "AutoGPT+ P: Affordance-based Task Planning with Large Language Models," *arXiv preprint arXiv:2402.10778*, 2024.
- [47] L. Guan, K. Valmeekam, S. Sreedharan, and S. Kambhampati, "Leveraging Pre-trained Large Language Models to Construct and Utilize World Models for Model-based Task Planning," *Advances in Neural Information Processing Systems*, vol. 36, pp. 79 081–79 094, 2023.
- [48] L. Wang, C. Ma, X. Feng, Z. Zhang, H. Yang, J. Zhang, Z. Chen, J. Tang, X. Chen, Y. Lin *et al.*, "A Survey on Large Language Model based Autonomous Agents," *Frontiers of Computer Science*, vol. 18, no. 6, p. 186345, 2024.
- [49] S. Hu, T. Huang, F. Ilhan, S. Tekin, G. Liu, R. Kompella, and L. Liu, "A Survey on Large Language Model-Based Game Agents," *arXiv preprint arXiv:2404.02039*, 2024.
- [50] X. Wang, Y. Chen, L. Yuan, Y. Zhang, Y. Li, H. Peng, and H. Ji, "Executable Code Actions Elicit Better LLM Agents," *arXiv preprint arXiv:2402.01030*, 2024.
- [51] B. Liu, Y. Jiang, X. Zhang, Q. Liu, S. Zhang, J. Biswas, and P. Stone, "LLM+P: Empowering Large Language Models with Optimal Planning Proficiency," *arXiv preprint arXiv:2304.11477*, 2023.
- [52] S. Sahoo and B. Choudhury, "A review of methodologies for path planning and optimization of mobile robots," *Journal of Process Management and New Technologies*, vol. 11, no. 1-2, pp. 122–140, 2023.
- [53] J.-P. Laumond, S. Sekhavat, and F. Lamiriaux, *Guidelines in Nonholonomic Motion Planning for Mobile Robots*. Springer Berlin Heidelberg, 2006, vol. 299, pp. 1–53.
- [54] X. Tong, C. Siwei, W. Dong, W. Ti, X. Yang, and Z. Weigong, "A Novel Path Planning Method for Articulated Road Roller Using Support Vector Machine and Longest Accessible Path With Course Correction," *IEEE Access*, vol. 7, pp. 182 784–182 795, 2019.
- [55] B. J. Alshaer, T. T. Darabseh, and M. A. Alhanouti, "Path planning, modeling and simulation of an autonomous articulated heavy construction machine performing a loading cycle," *Applied Mathematical Modelling*, vol. 37, no. 7, pp. 5315–5325, 2013.
- [56] T. Nayl, G. Nikolakopoulos, and T. Gustafsson, "Effect of kinematic parameters on MPC based on-line motion planning for an articulated vehicle," *Robotics and Autonomous Systems*, vol. 70, pp. 16–24, 2015.
- [57] J. Hu, F. Yang, F. Nan, and M. Hutter, "Motion Primitives Planning For Center-Articulated Vehicles," in *2024 IEEE/RSJ International Conference on Intelligent Robots and Systems (IROS)*, 2024, pp. 12 702–12 709.
- [58] N. Belov, C. E. V. Barbosa, F. Keppler, J. Kolb, G. Nitzsche, and S. Wagner, "TruckTriX® Path-Planning in the helyOS Operating System for Yard Automation," in *2021 IEEE 19th International Conference on Industrial Informatics (INDIN)*. IEEE, 2021, pp. 1–6.
- [59] Y. Bian, M. Yang, X. Fang, and X. Wang, "Kinematics and Path Following Control of an Articulated Drum Roller," *Chinese Journal of Mechanical Engineering*, vol. 30, no. 4, pp. 888–899, 2017.
- [60] D. Dolgov, S. Thrun, M. Montemerlo, and J. Diebel, "Path Planning for Autonomous Vehicles in Unknown Semi-structured Environments," *The International Journal of Robotics Research*, vol. 29, no. 5, pp. 485–501, 2010.
- [61] B. Molter and J. Fottner, "Semi-Automatic Pallet Pick-up as an Advanced Driver Assistance System for Forklifts," in *2019 IEEE Intelligent Transportation Systems Conference (ITSC)*, 2019, pp. 4464–4469.
- [62] L. Baglivo, N. Biasi, F. Biral, N. Bellomo, E. Bertolazzi, M. Da Lio, and M. de Cecco, "Autonomous pallet localization and picking for industrial forklifts: a robust range and look method," *Measurement Science and Technology*, vol. 22, no. 8, p. 085502, 2011.
- [63] E. Tsiogas, I. Kleitsiotis, I. Kostavelis, A. Kargakos, D. Giakoumis, M. Bosch-Jorge, R. J. Ros, R. L. Tarazon, S. Likothanassis, and D. Tzovaras, "Pallet detection and docking strategy for autonomous pallet truck AGV operation," in *2021 IEEE/RSJ International Conference on Intelligent Robots and Systems (IROS)*, 2021, pp. 3444–3451.
- [64] N. Kita and T. Kato, "Image Measurement Method for Automatic Insertion of Forks into Inclined Pallet," in *2022 17th International Conference on Control, Automation, Robotics and Vision (ICARCV)*, 2022, pp. 441–448.
- [65] S. Macenski, T. Foote, B. Gerkey, C. Lalancette, and W. Woodall, "Robot Operating System 2: Design, architecture, and uses in the wild," *Science Robotics*, vol. 7, no. 66, p. eabm6074, 2022.
- [66] F. R. Kschischang, B. J. Frey, and H.-A. Loeliger, "Factor Graphs and the Sum-Product Algorithm," *IEEE Transactions on Information Theory*, vol. 47, no. 2, pp. 498–519, 2001.
- [67] "Reprint of: Mahalanobis, P.C. (1936) "On the Generalised Distance in Statistics."," *Sankhya A*, vol. 80, no. 1, pp. 1–7.
- [68] StereoLabs, "ZED 2 stereo camera," <https://www.stereolabs.com/zed-2/>, 2025, [Accessed January 16, 2025].
- [69] X. Zhou, D. Wang, and P. Krähenbühl, "Objects as Points," *arXiv preprint arXiv:1904.07850*, 2019.
- [70] R. M. Haralick, C.-N. Lee, K. Ottenberg, and M. Nolle, "Review and Analysis of Solutions of the Three Point Perspective Pose Estimation Problem," *International Journal of Computer Vision*, vol. 13, no. 3, pp. 331–356, 1994.
- [71] M. Schwingshackl, F. F. Oberweger, and M. Murschitz, "Few-shot Structure-Informed Machinery Part Segmentation with Foundation Models and Graph Neural Networks," in *Proceedings of the Winter Conference on Applications of Computer Vision (WACV)*, February 2025, pp. 1989–1998.
- [72] J. Weichselbaum, C. Zinner, O. Gebauer, and W. Pree, "Accurate 3D-vision-based obstacle detection for an autonomous train," *Computers in Industry*, vol. 64, no. 9, pp. 1209–1220, 2013.
- [73] L. Fel, C. Zinner, T. Kadiofsky, W. Pointner, J. Weichselbaum, and C. Reisner, "ODAS-An anti-collision assistance system for light rail vehicles and further developments," in *7th Transport Research Arena TRA 2018*, 2018.
- [74] M. Ester, H.-P. Kriegel, J. Sander, and X. Xu, "A Density-Based Algorithm for Discovering Clusters in Large Spatial Databases with Noise," in *Proceedings of the Second International Conference on Knowledge Discovery and Data Mining (KDD-96)*. AAAI Press, 1996, pp. 226–231.
- [75] M. Colledanchise and P. Ogren, *Behavior Trees in Robotics and AI: An Introduction*. CRC Press, 2018.
- [76] D. Faconti and M. Colledanchise, "BehaviorTree.CPP," <https://github.com/BehaviorTree/BehaviorTree.CPP>, 2018, [Accessed January 2, 2025].
- [77] S. Macenski, T. Moore, D. Lu, A. Merzlyakov, and M. Ferguson, "From the desks of ROS maintainers: A survey of modern & capable mobile robotics algorithms in the robot operating system 2," *Robotics and Autonomous Systems*, p. 104493, 2023.
- [78] S. Zafari, F. Steiner, M. Huber, K. Kassem, P. Zips, and M. Tscheligi, "A gesture-based interactive system for automated material handling vehicles: Implementation and comparative study," in *Proceedings of the 12th International Conference on Human-Agent Interaction*, ser. HAI '24. New York, NY, USA: Association for Computing Machinery, 2024, p. 176–184.
- [79] S. Macenski, M. Booker, and J. Wallace, "Open-Source, Cost-Aware Kinetically Feasible Planning for Mobile and Surface Robotics," *arXiv preprint arXiv:2401.13078*, 2024.
- [80] Intel, "USB 3.0\* Radio Frequency Interference Impact on 2.4 GHz Wireless Devices," Intel Corporation, White Paper, 2012. [Online]. Available: <https://www.usb.org/sites/default/files/327216.pdf>